

A Novel Method to Identify AGNs based on Emission Line Excess and the Nature of Low-luminosity AGNs in the Sloan Digital Sky Survey II – Nature of Low-luminosity AGNs

Masayuki Tanaka

*Institute for the Physics and Mathematics of the Universe, The University of Tokyo
5-1-5 Kashiwanoha, Kashiwa-shi, Chiba 277-8583, Japan
masayuki.tanaka@ipmu.jp*

(Received ; accepted)

Abstract

We develop a novel method to identify active galactic nuclei (AGNs) and study the nature of low-luminosity AGNs in the Sloan Digital Sky Survey. This is the second part of a series of papers and we study the correlations between the AGN activities and host galaxy properties. Based on a sample of AGNs identified with the new method developed in Paper-I, we find that AGNs typically show extinction of $\tau_V = 1.2$ and they exhibit a wide range of ionization levels. The latter finding motivates us to use [OII]+[OIII] as an indicator of AGN power. We find that AGNs are preferentially located in massive, red, early-type galaxies. By carefully taking into account a selection bias of the Oxygen-excess method, we show that strong AGNs are located in actively star forming galaxies and rapidly growing super-massive black holes are located in rapidly growing galaxies, which clearly shows the co-evolution of super-massive black holes and the host galaxies. This is a surprising phenomenon given that the growths of black holes and host galaxies occur at very different physical scales. Interestingly, the AGN power does not strongly correlate with the host galaxy mass. It seems that mass works like a 'switch' to activate AGNs. The absence of AGNs in low-mass galaxies might be due the absence of super-massive black holes in those galaxies, but a dedicated observation of nuclear region of nearby low-mass galaxies would be necessarily to obtain deeper insights into it.

Key words: galaxies: active — galaxies: evolution — galaxies: fundamental parameters — galaxies: statistics

1. Introduction

Massive black holes were first speculated as powerhouses for luminous quasars (e.g., Lynden-Bell 1969). A large amount of work conducted afterwards vastly improved our understanding of active galactic nuclei (AGNs) and it is now widely recognized that super-massive black holes are far from rare, exotic objects and they are basic constituents of massive galaxies. A large spectroscopic survey of nearby galaxies has been a successful strategy to unveil statistical nature of AGNs. Ho et al. (1995) reported on a systematic survey of 486 nearby galaxies with the Hale 5m telescope and Ho et al. (1997) studied weak AGNs from the survey, most of which turned out to be low-ionization objects often called LINERs (Heckman 1980). They found that AGNs are preferentially located in massive early-type galaxies with large bulges. Further observations of nearby galaxies revealed that super-massive black hole mass correlates with host galaxy properties, particularly with bulge luminosity and mass (Kormendy & Richstone 1995; Magorrian et al. 1998; Ferrarese & Merritt 2000; Gebhardt et al. 2000). This suggests that the super-massive black hole growth and galaxy growth are linked, and it has motivated a lot of effort to study the black hole evolution in the context of galaxy evolution both theoretically and observationally.

Recent galaxy formation models, which incorporates energy feedback by AGNs in one way or another, seem to reproduce observed properties of galaxies reasonably well. AGNs seem to be a favorable energy feedback mechanism due to their contin-

uous energy output in massive galaxies with QSO-like strong feedback in starburst phase (e.g., Granato et al. 2004; Springel et al. 2005; Bower et al. 2006; Croton et al. 2006), which helps reproduce the 'break' in the massive end of the stellar mass function. However, these simulations cannot directly follow the AGN physics, which happens on less than a parsec scale, and rely on a simplified recipe. Also, the exact form of energy feedback is still highly uncertain. Despite the simplicity and assumptions employed, however, these models succeeded to reproduce overall properties of observed galaxies relatively well.

Observational evidence of AGN feedback, on the other hand, is still limited and we do not yet know how exactly AGN affects the galaxy evolution. High-quality large spectroscopic surveys of the local universe such as the 2dF survey (Colless et al. 2003) and the Sloan Digital Sky Survey (SDSS; York et al. 2000) rapidly improved our understanding of AGNs. It is now widely accepted that AGNs are preferentially located in massive galaxies (Kauffmann et al. 2003). Strong AGNs tend to reside in blue galaxies and high ionization AGNs (Seyferts) also slightly prefer blue galaxies over red galaxies (Kewley et al. 2006). It seems that very strong AGN activities may be affecting star formation activities of the host galaxies. Ho (2005) studied nearby QSOs and found possibly suppressed SFRs of the host galaxies. Kim et al. (2006) extended the analysis with a large number of type-I AGNs drawn from SDSS and suggested that the observed [OII] emission can be explained entirely by the photo-ionization due to AGN with little emission

from HII regions. Recently, Greene et al. (2011) examined 15 luminous QSOs and reached essentially the same conclusion. If we turn our attention to low-luminosity AGNs, which comprise the majority of the overall AGN population, some authors claimed that the host galaxies tend to show colors in between the red sequence and blue cloud (so-called green valley), which led them to speculate on on-going effects of AGN feedback (Schawinski et al. 2007; Schawinski et al. 2010). Heckman et al. (2004) studied the mass of the AGN host galaxies and suggested that most of the active super-massive black holes are located in intermediate mass galaxies, therefore representing down-sizing in AGN activities.

A significant fraction of the previous studies from the surveys of the local universe is based on optical emission line diagnostics first proposed by Baldwin et al. (1981; hereafter BPT) to identify AGNs thanks largely to a large number of high quality spectra from SDSS. However, a major drawback of the popular BPT diagnostics is that it requires four emission lines which are not always easy to measure at high signal-to-noise ratios. Among them, $H\beta$ can be fairly weak in AGNs and that imposes a practical limit on its sensitivity to low-luminosity AGNs (Paper-I). Several authors proposed variances of the BPT diagnostics to overcome the issue (Rola et al. 1997; Lamareille et al. 2004; Yan et al. 2006; Yan et al. 2011; Juneau et al. 2011), but they may not be fully satisfactory alternatives. In particular, some of them make a priori assumption of host galaxy properties and therefore may not be suited to study AGN - host galaxy correlations.

To improve the situation, we have developed a novel method to identify AGNs in Paper-I based on a very simple idea of comparing expected with observed emission line luminosities. We do not make any a priori assumptions of host galaxy properties. While the method suffers from contamination and incompleteness as all the other AGN identification methods do, it is a statistically efficient method to identify low-luminosity AGNs. With this new method, we aim to study the nature of low-luminosity AGNs and their host galaxy properties in this paper.

The structure of this paper is as follows. In Section 2, we give a brief overview of the new AGN identification method developed in Paper-I. We then develop a basis to characterize AGN activities in Section 3, followed by a detailed study of correlations between AGN activities and host galaxy properties in Section 4. We summarize our results and discuss their implications in Section 5. Unless otherwise stated, we adopt $\Omega_M = 0.3$, $\Omega_\Lambda = 0.7$, and $H_0 = 70 \text{ km s}^{-1} \text{ Mpc}^{-1}$. All the magnitudes are given in the AB system. We use the following abbreviations : AGN for active galactic nucleus, BPT for the Baldwin et al. (1981) diagnostics, SF for star formation and SFR for star formation rate. Emission lines used in this work include [OII] $\lambda\lambda 3726, 3729$, $H\beta$ $\lambda 4861$, [OIII] $\lambda 5007$, [OI] $\lambda 6300$, $H\alpha$ $\lambda 6563$, [NII] $\lambda 6583$, and [SII] $\lambda 6716, 6730$.

2. Overview of the new method and the data

2.1. Method

We briefly give an overview of the new method to identify AGNs. For the full development, readers are referred to Paper-I.

The most widely adopted optical emission line diagnostics to identify AGNs is the one proposed by Baldwin et al. (1981) and later extended by Veilleux & Osterbrock (1987). It is based on the idea that an ionizing spectrum of AGN is often harder than that of young stars, and emission lines show characteristic intensity ratios. However, in principle, a single emission line contains information about AGN. An emission line luminosity of a galaxy we measure from its spectrum is

$$L_{measured} = L_{SF} + L_{AGN}, \quad (1)$$

where L_{SF} and L_{AGN} are luminosities due to star formation and AGN, respectively. It has been a long standing problem to separate the two components, which has hindered detailed studies of pure AGN emission. But, we have developed a novel method to estimate L_{SF} in Paper-I. AGNs often emit strong emission lines, but their continuum is generally much weaker. Optical continuum emission of a galaxy spectrum is dominated by stellar light, not by AGN, in most AGNs (Schmitt et al. 1999). The stellar continuum contains information about star formation rates (SFRs) and dust extinction of the galaxy. We extract these two pieces of information by fitting model templates generated with an updated version of the Bruzual & Charlot (2003) code to the observed spectrum. From SFRs and dust extinction, we can work out L_{SF} . We then compare $L_{measured}$ with L_{SF} . If we observe a significant L_{AGN} , a galaxy likely hosts an AGN. As we will discuss in Section 3, AGNs exhibit a wide range of ionization state and we use a sum of [OII] and [OIII] luminosities to identify AGNs. We have shown that we can estimate L_{SF} for [OII]+[OIII] with a factor of ~ 1.7 accuracy in Paper-I. Since we identify AGNs using excess Oxygen emission, we dub the method ‘‘Oxygen-excess method’’. Note that we will extensively use stellar mass, SFR and dust extinction from the spectral fits in this paper.

Compared to the commonly used Baldwin et al. (1981) diagnostics, this Oxygen-excess method gives the same SF/AGN classifications for 85% of objects that exhibit strong enough emission lines to apply the BPT method. The BPT diagnostics uses 4 emission lines and it takes ratios of them, requiring a high signal-to-noise ratio for each line. On the other hand, the new method uses a sum of the two lines and its requirement for signal-to-noise is less demanding. As a result, the method is applicable to 78% of the objects in our sample, while BPT is applicable only to 43%. Our method is thus fairly sensitive to low-luminosity AGNs. We have quantified average properties of the Oxygen-excess objects by stacking the spectra and we have shown that many of the Oxygen-excess objects, if not all, likely host AGNs. Serendipitous X-ray observations (Evans et al. 2010) as well as radio data from the FIRST survey (Becker et al. 1995; White et al. 1997) also show that SF/AGN classifications are made well. Another unique feature of the method is that it allows us to subtract emission line luminosities due to star formation and extract AGN luminosities, which are crucial to characterize AGNs. We will make a full use of these unique features to study the nature of low-luminosity AGNs in this paper.

2.2. Data

We use data from the Sloan Digital Sky Survey Data Release 7 (Abazajian et al. 2009). Using a dedicated 2.5m telescope

(Gunn et al. 2006), the SDSS surveyed a quarter of the sky in both imaging and spectroscopy (Fukugita et al. 1996; Gunn et al. 1998; Eisenstein et al. 2001; Strauss et al. 2002; Richards et al. 2002; Gunn et al. 2006; Doi et al. 2010). The galaxy sample for our study is drawn from the main galaxy sample (Strauss et al. 2002), which is a flux-limited sample down to $r = 17.77$ selected from the imaging survey. We apply the following selection criteria: SPECCLASS=2 (i.e., objects are galaxies) located at $0.02 < z < 0.10$ with high confidence flags ($z\text{CONF} > 0.8$ and $z\text{WARNING} = 0$). We intentionally remove QSO-like objects (SPECCLASS=3) because our method is not applicable to those objects (continuum needs to be dominated by stars, not by AGN), leaving 283,031 objects in total. We apply a first-order correction for the fiber loss to the stellar mass and SFR by assuming that light in the fiber is representative of the entire galaxy. The corrected quantities are shown with a subscript *apercorr*.

2.3. Caveats on photo-ionization due to non-AGN sources

Before we present our results, it is important to remind of the contamination of objects that are photo-ionized by non-AGN sources. As discussed in Paper-I, there are a number of possible non-AGN sources that could produce LINER-like emission line ratios. They include shocks (Cox 1972; Heckman 1980; Dopita & Sutherland 1995; Dopita & Sutherland 1996), Wolf-Rayet stars (Terlevich & Melnick 1985; Kewley et al. 2001), post-starburst (Taniguchi et al. 2000) and post-AGB stars (Binette et al. 1994; Stasińska et al. 2008; Sarzi et al. 2010; Cid Fernandes et al. 2011). Relative contributions of these ionizing sources to the observed LINER populations are uncertain, but they may contaminate our AGN sample.

As shown later, most of the Oxygen-excess objects are red, massive galaxies. In these galaxies, shocks, Wolf-Rayet stars, and post-starburst are unlikely the primary origin of the observed emission. Post-AGB stars remain a concern. Several attempts have been made to quantify their role (Binette et al. 1994; Stasińska et al. 2008; Sarzi et al. 2010; Cid Fernandes et al. 2011; Yan & Blanton 2011). In particular, Sarzi et al. (2010) and Yan & Blanton (2011) studied nearby galaxies and observed spatially extended $H\alpha$ or $H\beta$ emission, which is unlikely to be fully explained by a central source. There is no doubt that these post-AGB stars contaminate the true AGN population and the observed emission line luminosities of the Oxygen-excess objects are at least partly contaminated by post-AGB photo-ionization.

We argue in Section 3.3 that emission due to post-AGB stars does not seem to dominate the overall emission, but the exact fraction of objects that are photo-ionized by post-AGB stars among the Oxygen-excess objects and the exact contribution of post-AGB stars to the observed emission remain unclear. As discussed in Paper-I, the SDSS data are not a right data set to precisely pin down the role of post-AGB stars and we do not try to pursue the issue further in this paper. But, we should bear in mind that this unknown role of post-AGB stars remains one of the major uncertainties throughout the paper.

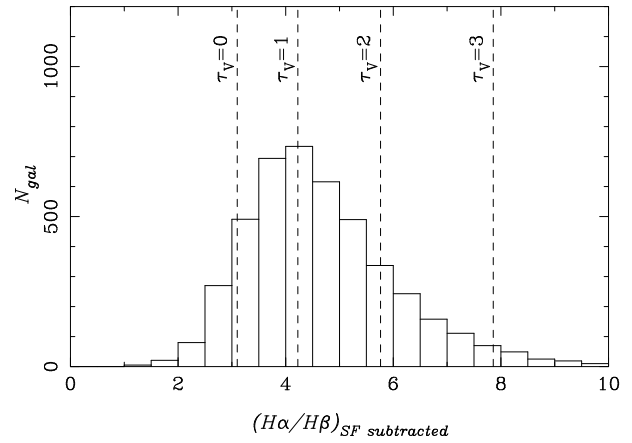


Fig. 1. Distribution of the Balmer decrement. The star formation component is subtracted from the $H\alpha$ and $H\beta$ luminosities and extinction due to the interstellar medium is corrected for. The dashed lines show τ_V assuming the dust-free Balmer decrement of 3.1. Note that one can convert τ_V into the commonly used extinction in the V -band using $A_V = 1.09\tau_V$. We use objects with $H\alpha$ and $H\beta$ detected at more than 10σ only here to quantify the line ratio.

3. Dust in AGNs and AGN power indicator

First of all, we develop a basis to characterize AGN activities. We first quantify dust extinction in AGNs. We then study emission line properties using the extinction corrected luminosities and examine indicators of the AGN power. Finally, we revisit the issue of measuring SFRs of the host galaxies from emission lines.

3.1. Extinction in AGNs

AGNs can be obscured by dust around the nuclear regions and it is essential to correct for the dust extinction in order to quantify AGN activities. We measure emission line luminosities due to AGNs in a two-step procedure. First, we subtract the star formation component, L_{SF} , from a measured emission line luminosity. We then correct for the dust extinction to obtain emission line luminosities coming out of the central region. To be specific, in case of $H\alpha$,

$$L_{H\alpha} = (L_{H\alpha,meas} - L_{H\alpha,sf}) \times \exp(0.3 \times 0.75 \times \tau_V), \quad (2)$$

where $L_{H\alpha,meas}$, $L_{H\alpha,sf}$ and τ_V are the measured $H\alpha$ luminosity, 'predicted' $H\alpha$ luminosity due to star formation, and the optical depth in the V -band from the spectral fitting. The factor of 0.3 to τ_V is due to the assumption that 30% of the dust extinction comes from the ambient interstellar medium (Charlot & Fall 2000). The term $0.75\tau_V$ is the optical depth at the wavelength of $H\alpha$ assuming the Cardelli et al. (1989) extinction curve. We note that we tend to underestimate τ_V from the spectral fitting (see Fig. 1 of Paper-I) and the extinction due to the interstellar medium may not be fully corrected¹.

We apply the same equation to $L_{H\beta}$ and plot the Balmer decrement of the AGN emissions in Fig. 1. Here we adopt

¹ We underestimate τ_V systematically by $\Delta\tau_V \sim 1$ for most objects as shown in Fig.1 of Paper-I. If we empirically correct for the offset, we obtain a median AGN extinction of $\tau_V = 0.7$, which is smaller than that obtained below ($\tau_V = 1.2$).

the dust-free Balmer decrement of 3.1 for AGNs (Halpern & Steiner 1983; Ferland & Netzer 1983; Gaskell & Ferland 1984). We also have confirmed that there is no change in our main conclusions if we adopt a decrement of 2.86 (case 'B' recombination for $T = 10^4$ K and $N_e = 10^{12}$ cm $^{-3}$; Osterbrock & Ferland 2006). The Oxygen-excess objects typically have $\tau_V = 0 - 2$ extinction with the median being $\tau_V = 1.2$. We note that the median value does not change if we include lower significance detections of the lines (e.g., 3σ), although the scatter significantly increases. Dahari & De Robertis (1988) showed that Seyfert 2's typically show the Balmer decrement of 3 - 6, which is fully consistent with our estimates here. Kauffmann et al. (2003) quoted a median extinction of $A_V \sim 3$ mag. in AGNs using data from SDSS. Our extinction is less than that, but their large value is due to the assumption of the relatively flat extinction curve of Charlot & Fall (2000). We have confirmed that we obtain a similar amount of extinction if we use the Charlot & Fall (2000) curve. It is interesting to note that the observed range of Balmer decrement is similar to that observed in Seyfert galaxies (Osterbrock 1977; Greene & Ho 2005).

For the Balmer decrement measurements, we need good signal-to-noise ratios on the Balmer lines, but $H\beta$ can often be noisy (and that is the reason why the BPT diagnostics is not applicable for a large number of galaxies). It is difficult to measure the Balmer decrement for individual galaxies and we therefore apply a constant extinction correction regardless of the properties of the AGNs and host galaxies. We note that we do not observe strong dependence of the balmer decrement on AGN power and thus the constant correction is a reasonable first order correction. The total optical depth of Oxygen-excess objects is

$$\tau_{V,total} = 0.3 \times \tau_V + 1.2. \quad (3)$$

The first term is the extinction due to the ambient interstellar medium, which is derived from the spectral fitting. The second term is the extinction around the nuclear region. To be specific, we replace $0.3 \times \tau_V$ in Eq. 2 with Eq. 3 to obtain intrinsic line luminosities due to AGN. We use a subscript *AGN* when we show star formation subtracted, extinction corrected emission line luminosities of the Oxygen-excess objects. This is just for simplicity and we do not mean that all of the Oxygen-excess objects are real AGNs.

3.2. A new indicator of AGN power and comparisons with X-ray power

Having quantified extinction in AGNs, we are now ready to characterize AGN activity. In order to quantify AGN power, we ideally want to integrate all the photons emitted from the central engine over the whole wavelength range. But, this is observationally very challenging to achieve. A luminosity of the [OIII] line is often used as an indicator of AGN power and a clear correlation between the absorbed [OIII] luminosity and hard X-ray luminosity has been observed in a hard X-ray selected sample (Heckman et al. 2005). Recently, de Gasperin et al. (2011) also presented a tight correlation between absorbed hard X-ray luminosity and [OIII] luminosity. The use of [OIII] as a proxy for AGN power is partly motivated by a commonly adopted assumption that contamination from star formation is relatively small in [OIII]. But, [OIII] is a relatively high ion-

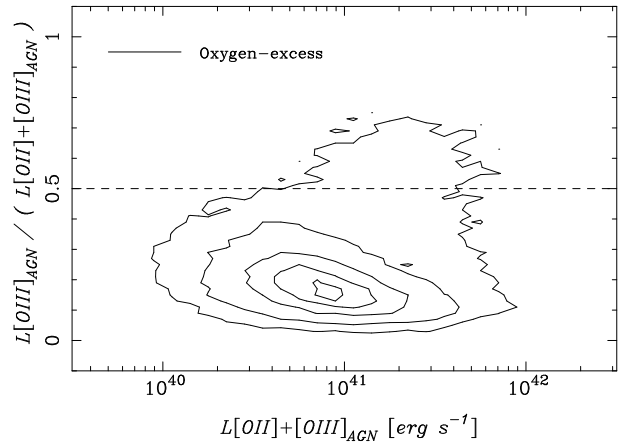


Fig. 2. Fraction of [OIII] $_{AGN}$ luminosity to [OII] $_{AGN}$ + [OIII] $_{AGN}$ luminosity plotted against [OII] $_{AGN}$ + [OIII] $_{AGN}$. The solid contours are Oxygen-excess objects and their star formation fluxes are subtracted off and the extinction is corrected for using Eq. 3. The horizontal dashed line shows the equality of [OII] $_{AGN}$ and [OIII] $_{AGN}$ luminosities. [OII] $_{AGN}$ <[OIII] $_{AGN}$ holds above the line, and [OII] $_{AGN}$ >[OIII] $_{AGN}$ holds below the line.

ization line. Is it a good indicator of AGN power for low-luminosity AGNs studied here?

If we look at ionization state of the Oxygen-excess galaxies in Fig. 2, we find that AGNs spans a wide range in ionization state. Heckman (1980) first introduced a class of low-ionization emission line galaxies (LINERs). The original definition of LINERs is [OII]>[OIII] and [OI]> 0.33[OIII]. Ho et al. (1993) showed that this definition is essentially the same as [OIII]/ $H\beta$ > 3. Due to the weak $H\beta$ emission in most of the Oxygen-excess galaxies, we further revise the definition to [OII] $_{AGN}$ >[OIII] $_{AGN}$, which is equivalent to [OIII]/ $H\beta$ > 3 due to the tight correlation between [OII]/[OIII] and [OIII]/ $H\beta$ (Baldwin et al. 1981). Note that we use star formation subtracted, extinction corrected luminosities for the LINER/Seyfert classification. At low luminosities, AGNs are mostly LINERs. Seyfert-like galaxies with [OII] $_{AGN}$ <[OIII] $_{AGN}$ appear at high luminosities. We find that 7% of the Oxygen-excess objects have [OII] $_{AGN}$ <[OIII] $_{AGN}$. This fraction should not be taken as a general fraction of Seyferts among AGNs because we intentionally excluded QSO-like objects from the sample.

[OIII] is often used as an indicator of AGN power (Heckman et al. 2005), but given the relatively wide range of ionization states of the Oxygen-excess objects, we deem that the sum of [OII]+[OIII] is a better indicator of the AGN power. In general, [OII] and [OIII] lines balance each other in gaseous nebulae. [OIII] is strong in high ionization states and [OII] is strong in low ionization states. A sum of the two lines is more robust to variations in ionization levels than either one of them and is a better indicator of total energy emitted by Oxygen. $H\alpha$ line would be another straightforward option. However, as shown in Paper-I, AGNs exhibit relatively weak $H\alpha$ and the AGN component does not stand out. If we subtract the star formation component as we do for [OII] and [OIII], we obtain a negative $H\alpha$ luminosity for a number of Oxygen-excess objects. This means that our SFR and τ_V estimates from the

spectral fits are not sufficiently good to extract the relatively weak $H\alpha$ due to AGN. On the other hand, the collisionally excited lines are normally strong in AGNs. For these reasons, we choose $[\text{OII}]+[\text{OIII}]$ to identify AGNs and to characterize them. If one could improve the estimates of $H\alpha$ flux due to star formation, $H\alpha$ would be a better indicator because it is less sensitive to ionization, dust, and metallicity.

We now test this new indicator of the AGN power by comparing with hard X-ray luminosities, which is likely a very good indicator of the AGN power (Ho 2008). As described in Paper-I, we use the Chandra-SDSS matched catalog release 1.1 (Evans et al. 2010). We require the sources to be point-like and located within 2 arcsec from the optical center to ensure that X-rays likely originate from the center of the galaxies. We compare the optical emission line luminosities with X-ray luminosities to verify the effectiveness of the new AGN power indicator. We note that we remove X-ray sources that may be non-AGN origin from the comparisons (Fig. 11 of Paper-I show how we identify those sources). We further note that we do not correct for absorption in hard X-rays. The typical Galactic neutral hydrogen column density in our sample is low (a few times 10^{20}cm^{-2} ; Dickey & Lockman 1990) and intrinsic absorption is likely below 10^{22}cm^{-2} within the luminosity range we explore here (Mainieri et al. 2007). At this column density, absorption in the hard band is small (Morrison & McCammon 1983). Our hard X-ray luminosity should therefore be a reasonable estimate.

We show comparisons between hard X-ray luminosity and optical emission line luminosities in Fig. 3. We show not only $[\text{OII}]+[\text{OIII}]_{\text{AGN}}$, but $[\text{OII}]_{\text{AGN}}$ and $[\text{OIII}]_{\text{AGN}}$ as well. We find that all the lines show statistically significant correlations with X-rays. We perform the Spearman’s rank test and find the positive correlation with a high significance ($> 2\sigma$) to reject the null hypothesis in all the lines. Also, we perform the biweight fits to the data points and show the best-fitting lines in the plots. The dominant source of error in our AGN flux estimates is in our prediction of emission line fluxes due to star formation, which is 0.23 and 0.29 dex for $[\text{OII}]$ and $[\text{OIII}]$, respectively. We adopt it as an uncertainty in the subtraction of the star formation component for each line. The biweight fits are performed taking these uncertainties into account. We find that $[\text{OIII}]_{\text{AGN}}$ shows a stronger correlation with the X-ray power than $[\text{OII}]_{\text{AGN}}$ (Simpson 1998). Contrary to our expectations, $[\text{OII}]+[\text{OIII}]_{\text{AGN}}$ shows somewhat poorer correlation than $[\text{OIII}]_{\text{AGN}}$ alone, although the scatter decreases slightly. Apparently, the relatively poor correlation between $[\text{OII}]_{\text{AGN}}$ and X-ray luminosities weaken the correlation in $[\text{OII}]+[\text{OIII}]_{\text{AGN}}$. We suspect that it might be due to insufficient extinction correction. Due to our limited ability to measure the extinction in individual galaxies, we apply the constant correction for dust due to AGN to all the galaxies. But, this is probably just a rough correction and a small over/under correction introduces a larger error in $[\text{OII}]$ than in $[\text{OIII}]$ because $[\text{OII}]$ is at a shorter wavelength.

Now, we face a difficult question of the choice of the AGN power indicator. We would like to use $[\text{OII}]+[\text{OIII}]$ to keep consistency with the identification method. As shown in Fig. 7 of Paper-I, the stacked spectra of the Oxygen-excess objects show stronger $[\text{OII}]$ than $[\text{OIII}]$ and $[\text{OII}]$ is a very powerful

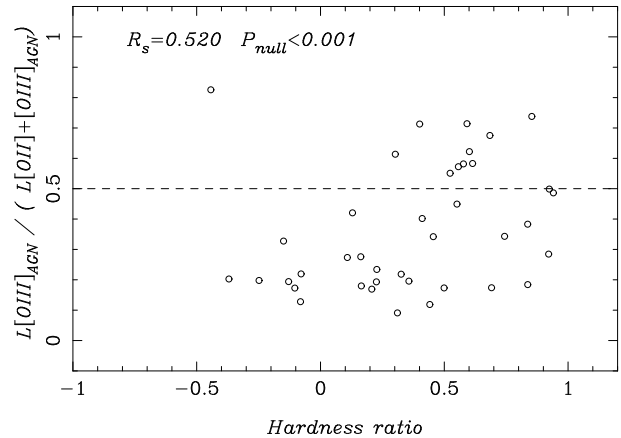


Fig. 4. $[\text{OIII}]_{\text{AGN}}/([\text{OII}]_{\text{AGN}}+[\text{OIII}]_{\text{AGN}})$ plotted against X-ray hardness ratio between soft (0.5-1.2 keV) and hard (2-7keV) bands. The numbers show a Spearman’s rank correlation coefficient and a null probability.

feature to identify Oxygen-excess objects. On the other hand, we would like to use $[\text{OIII}]$ only as a better indicator of the AGN power at the cost of losing consistency with the identification process somewhat. We have performed all the analyses presented in the paper using the two AGN power indicators and found that our conclusions remain totally the same regardless of the choice of the indicator. Given this robustness of our conclusions, we choose $[\text{OII}]+[\text{OIII}]$ as an indicator of the AGN power to keep the consistency with the AGN identification scheme.

We note in passing that we find an interesting correlation between “optical hardness” and X-ray hardness in Fig. 4. The optical line ratio plotted is essentially a simple function of $[\text{OII}]/[\text{OIII}]$, which is tightly correlated with $[\text{OIII}]/H\beta$ and is a good indicator of the ionization level (Baldwin et al. 1981). The Spearman’s rank correlation coefficient suggests a positive correlation between the optical and X-ray hardness with a statistically significant probability to reject the null hypothesis. This correlation can be understood as a product of two other correlations: one between L_X and hardness, and the other between emission line luminosity (which is correlated with L_X) and ionization state. We find that most of the hard sources in Fig. 4 are powerful AGN with $L_X > 10^{41.5}\text{erg s}^{-1}$. The AGN power then correlates with the ionization state as we will show in Section 4. These two correlations result in the trend in Fig. 4.

3.3. Possible evidence against a dominant role of post-AGB photo-ionization

Let us go back to the issue of objects with non-AGN photo-ionization. As we discussed in Paper-I and earlier in this paper, photo-ionization due to post-AGB stars can be important in LINERs. This comes from a few observational pieces of evidence. One is an energy budget argument. AGNs in LINERs tend to show a deficit in the amount of ionizing photons to fully explain the observed emission line luminosity (Maoz et al. 1998; Eracleous et al. 2010), requiring an additional source of ionization mechanism other than AGN. Another piece of evidence is that spatially extended emission is observed in

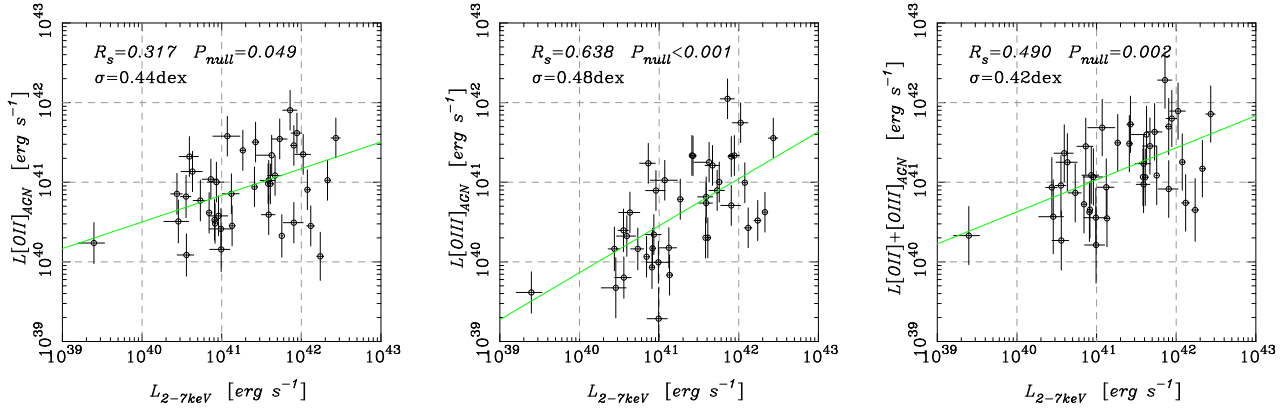


Fig. 3. Optical emission line luminosities plotted against hard X-ray luminosity. The plots show $[OII]_{AGN}$, $[OIII]_{AGN}$, and $[OII]+[OIII]_{AGN}$ from left to right. We remove soft low- L_X sources, some of which may not be AGNs, from the plots. The numbers in each plot show a Spearman’s rank correlation coefficient and a null probability. The solid lines are biweight fits to the data points and the dispersion in the optical luminosity around them are also shown in the plots.

LINERs using 2D spectrograph (Sarzi et al. 2010). Recently, Yan & Blanton (2011) also detected extended emission by a clever analysis of extended emission using varying redshift slices. We suspect that they suffer from contamination of star forming galaxies because a cut in D_{4000} is not enough to eliminate them from their sample as we mention below. Extended emission does not necessarily support the post-AGB origin of the emission (Yan & Blanton 2011), but spatially extended post-AGB stars remain a natural explanation of it. It is not clear whether post-AGB stars alone can produce enough ionizing photons to fully explain the observed emission (e.g., Yan & Blanton 2011 reports on the deficit of ionizing photons even if they assume that 100% of the ionizing photons are absorbed to produce emission line, while Sarzi et al. 2010 claims that they have enough ionizing photons). But, there is no doubt that emission due to post-AGB stars contaminate the emission line luminosities observed in the Oxygen-excess objects. The question is how much post-AGB stars contribute to the overall emission. To address this question, we focus on the correlation between optical emission line luminosities and hard X-ray luminosities in Fig. 3.

Post-AGB stars are not luminous in hard X-rays and the observed hard X-ray luminosity is likely primarily due to AGNs. One may worry that low-mass X-ray binaries may contribute to the hard X-ray luminosity. But, we show in Fig. 5 that the hard X-ray luminosity does not correlate with host galaxy stellar mass. The Spearman’s rank correlation coefficient is very small and the test does not reject the null hypothesis. This rather weak (or no) dependence of X-ray luminosity and host galaxy mass has also been noted by other authors (Mullaney et al. 2012; Aird et al. 2011). This strongly rules out the low-mass X-ray binary origin of the hard X-ray (Kim & Fabbiano 2004). The observed hard X-ray luminosity is primarily due to AGNs.

On the other hand, optical emission can be contaminated by post-AGB photo-ionization. The correlation between optical emission line luminosity and hard X-ray luminosity can therefore be used to gauge the contamination from post-AGB stars. The observed clear correlation between them shown in Fig. 3 suggests that the post-AGB contamination is not significant.

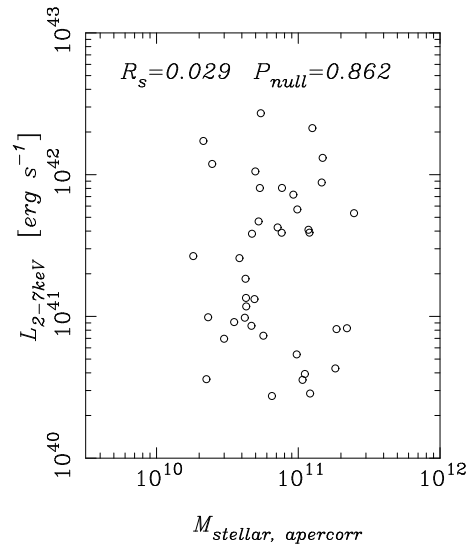


Fig. 5. Hard X-ray luminosity plotted against stellar mass. Objects that are likely contaminated by non-AGN sources (those in the dashed box in Fig. 11 of Paper-I) are removed. We also show the Spearman’s rank correlation coefficient and null probability.

If the contamination was significant, we would not have observed such a clear correlation between hard X-ray and, e.g., $[OII]+[OIII]$ luminosities. We shall note that the X-ray sources are drawn from serendipitous Chandra observations and they have typical properties of the Oxygen-excess objects, i.e., they are massive galaxies with $> 10^{10}M_{\odot}$ in stellar mass and are red quiescent galaxies with SFRs below $0.1M_{\odot} \text{ yr}^{-1}$. Therefore, these X-ray sources should be representative of the Oxygen-excess objects.

The X-ray sample is a small subset of the entire Oxygen-excess objects. To further quantify the emission due post-AGB stars, we define a subsample of the Oxygen-excess objects located at $0.055 < z < 0.060$ and with zero SFRs from the spectral fits. The narrow redshift slice is adopted to minimize the variation of our sensitivity to emission line luminosities within the redshift slice. The redshift range is arbitrarily chosen, but

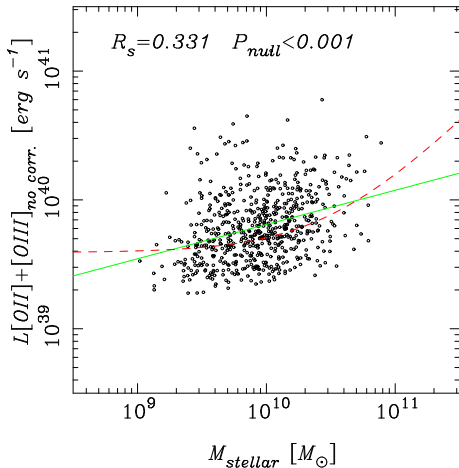


Fig. 6. [OII]+[OIII] luminosity plotted against stellar mass. The Oxygen-excess objects plotted here are located at $0.055 < z < 0.060$ and are not forming stars. Extinction defined in Eq. 3 is not applied and thus the luminosity is a ‘raw’ luminosity. Stellar mass is not corrected for the aperture loss. The solid line is a biweight fit to the data with a power-law slope of 0.26. The dashed curve shows the best fit model to the data (see text for details).

our conclusion below does not strongly depend on a particular choice of the redshift range. The zero SFR is to ensure that the host galaxies are not forming stars so that we do not have to correct for emission line luminosities due to star formation. The observed emission is therefore due to AGN and to post-AGB star photo-ionization (if present) in this subsample.

We show [OII]+[OIII] luminosity against stellar mass of this subsample in Fig. 6. Here, we do not apply any dust correction or aperture correction, i.e., ‘raw’ emission line luminosity within the fiber aperture is plotted against stellar mass within the fiber. The emission due to post-AGB stars should correlate strongly with stellar mass contained within the same area covered by the fibers. On the other hand, the AGN emission is unlikely to be strongly correlated with mass. Therefore, the correlation in Fig. 6 is a rough measure of the contribution of the post-AGB stars.

The Spearman’s rank test suggests that there is a correlation between the emission line luminosity and stellar mass. The null hypothesis is rejected at a significant level. This suggests that the post-AGB stars do contribute to the observed line luminosities. However, the observed correlation is relatively weak – the biweight fit gives a log-linear slope of 0.26. That is, if stellar mass increases by an order of magnitude, the emission line luminosity increases by less than a factor of 2. The abundance of post-AGB stars should depend on star formation histories of galaxies, which then depend on galaxy mass. However, we are looking only at massive quiescent galaxies², and it is very unlikely that their star formation histories vary so widely that the stellar mass dependence of the post-AGB abundance is smoothed out. The most naive interpretation of Fig. 6 would be that post-AGB stars do contribute to the observed line emis-

² Stellar mass plotted in Fig. 6 is not corrected for the aperture loss and is significantly smaller than a typical stellar mass of the Oxygen-excess objects discussed later in this paper, which is corrected for the aperture loss.

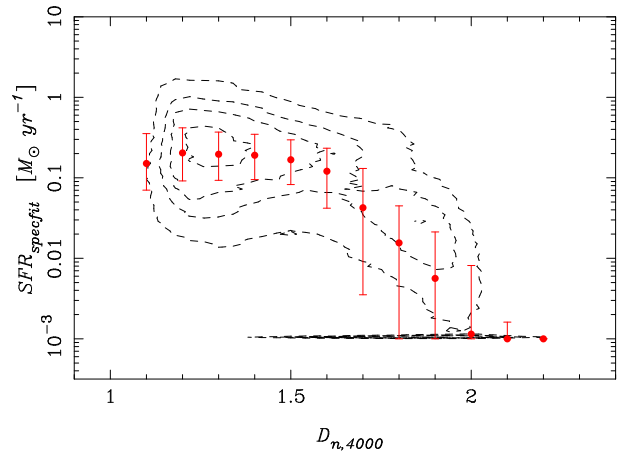


Fig. 7. SFR plotted against $D_{n,4000}$. The contours are all the objects in our parent sample (i.e., Main galaxies at $0.02 < z < 0.10$). The points and error bars show the median and quartile of the SFR distribution.

sion, but their contribution is minor.

Let us make an attempt to quantify the contribution of post-AGB stars using a very simple model. If we assume that emission due to post-AGB stars linearly increase with stellar mass and emission due to AGN does not depend on stellar mass, we can write

$$L_{obs} = L_{AGN} + \alpha \times M_{stellar}, \quad (4)$$

where L_{obs} , L_{AGN} , α are observed luminosity, luminosity due to AGN, and luminosity due to post-AGB photo-ionization per unit stellar mass. Let us modify the second term to define post-AGB emission relative to L_{AGN} at $M_{stellar} = 10^{10} M_{\odot}$.

$$L_{obs} = L_{AGN} \left(1 + \beta \times \frac{M_{stellar}}{10^{10} M_{\odot}} \right). \quad (5)$$

If $\beta = 1$, AGN and post-AGB equally contribute to the observed emission at $M_{stellar} = 10^{10} M_{\odot}$. We allow L_{AGN} and β to vary and fit the observed data in Fig. 6 using the χ^2 statistics. We find $\log L_{AGN} = 39.707 \pm 0.005$ and $\beta = 0.305 \pm 0.011$ give the best fit. The errors are derived by taking $\Delta\chi^2 = 1$ and are very small, but we should note that we ignore intrinsic scatter in L_{AGN} . The best-fit model is shown as the dashed curve in the figure. The fit suggests that 23% of the observed emission is due to post-AGB stars at $M_{stellar} = 10^{10} M_{\odot}$. Because of the assumptions we made, this is nothing more than a rough guess. But, it seems that post-AGB stars do not play a dominant role.

This result may not appear consistent with those from the literature (e.g., Sarzi et al. 2010; Yan & Blanton 2011). We do not try to resolve the issue as the SDSS data is unlikely a right data set to address it as we mentioned in Paper-I, but we shall recall that our concern is in a very low luminosity regime. We have to be sure that we do not suffer from low-level star formation that could happen in early-type galaxies. To illustrate its importance, we show SFR against $D_{n,4000}$ in Fig. 7. $D_{n,4000}$ is a sensitive index to age of the stellar population and is used in earlier work to select quiescent galaxies. However, it is hard to construct a pure sample of quiescent galaxies with this index alone. Even if galaxies have a large $D_{n,4000}$, they may well be

undergoing low-level star formation as shown in the figure. A SFR of $0.01 M_{\odot} \text{ yr}^{-1}$ translates into $L_{H\alpha} = 2 \times 10^{39} \text{ erg s}^{-1}$ (assuming no extinction by dust), which is a level of emission line luminosity that previous work reported. Such star formation is likely spatially extended. A careful removal of low-level star formation would be necessarily to put a better constraint on the role of post-AGB stars.

To summarize, emission line luminosities due to post-AGB photo-ionization seems to be a minor component of the overall luminosities. However, other authors claim a substantial role of post-AGB stars (Sarzi et al. 2010; Cid Fernandes et al. 2011; Yan & Blanton 2011). This issue remains unresolved and further effort is needed to settle it. One difficulty that hampers a clear conclusion is our limited understanding of the last stage of the stellar evolution. Another difficulty is the lack of suitable observational data to address the issue. Dedicated observations would be essential. For these difficulties, we cannot try to pursue the issue further in this paper, but we should bear in mind the potentially non-negligible contamination from post-AGB stars. Given the unclear (but likely minor) role of post-AGB stars, we do not correct for their contamination to the observed emission line luminosities throughout the paper. We assume that the observed emission is entirely due to AGN and SF.

3.4. Comparisons with radio power

We turn our attention to radio sources. We cross-matched our objects with FIRST (Becker et al. 1995; White et al. 1997) within 1 arcsec apertures as described in Paper-I to compare optical power with radio power. We miss extended radio lobes/jets, but extended radio sources constitute only 10% of the radio galaxies and hence should not strongly affect our results here (Lin et al. 2010). Also, extended radio lobes may not be a good measure of instantaneous AGN activity. We use $f_{\text{integrated}}$ from the FIRST catalog. Our results remain the same if we use f_{peak} .

We plot the optical power against radio power in Fig. 8. Note that we remove radio sources that are dominated by star formation from the comparisons (Fig. 13 of Paper-I shows how we identify star formation dominated sources). We observe a weak correlation between optical and radio and the Spearman's rank test rejects the null hypothesis. The weak correlation is in contrast to X-rays, which show stronger correlations. The loose radio-optical correlation may appear inconsistent with previous studies (e.g., Saunders et al. 1989; Baum & Heckman 1989; Rawlings & Saunders 1991; Hes et al. 1993; Ho 1999). These authors observed a relatively tight correlation between optical emission and radio power over a range of AGN types.

We do not consider our finding inconsistent with earlier findings for two reasons. First, our radio galaxy sample has more than an order of magnitude lower radio power than most of the previous studies. Majority of the Oxygen-excess objects are low-luminosity AGNs, while the previous studies focused on powerful radio galaxies. We are therefore not looking at the same population. Second, we exclude sources that are strongly contaminated by underlying star formation activities, while the previous studies did not. We find that the correlations slightly tighten up if we include those sources because we include the strong SFR-radio power correlation in the statistics. Our result may still not be consistent with observations by Ho (1999),

who studied nearby low-luminosity AGNs in early-type galaxies, in which the underlying star formation is probably not very strong. However, their early-type galaxy sample shows a large scatter comparable to ours (see their Fig. 2). For these reasons, we do not consider that our results are in strong conflict with previous studies. Recently, de Gasperin et al. (2011) observed no clear correlation between radio and X-ray powers. This probably suggests that there is no strong correlations between radio and optical powers in consistent with our result here.

The positive correlation shows the black hole activities and radio activities are weakly correlated in the Oxygen-excess objects under study. We note that several objects are detected both in X-rays and radio. We compare the X-ray and radio powers and find no significant correlations. Our statistics is very poor, but the observed lack of correlation is consistent with de Gasperin et al. (2011). The optical and X-ray powers are likely a good indicator of on-going AGN activities, while the radio power is likely not.

3.5. Is [OII] an indicator of SFRs of AGN host galaxies?

The [OII] emission is sometimes used as a proxy for host galaxy SFRs of high ionization AGNs such as Seyferts because this line is not very strong in those AGNs (e.g., Ho 2005). It may be reasonable to assume that [OII] is due to star formation in Seyfert galaxies, but is it still good for LINERs? The newly developed method allows us to statistically separate star formation and AGN components of a given emission line. We take this opportunity to quantify how well [OII] is correlated with SFRs over a range of AGN power and ionization states.

Fig. 9 shows the fractional contribution of [OII] due to star formation to the overall [OII] luminosity as a function of SFRs of the host galaxies (left panel), AGN power (middle panel), and ionization level (right panel). We do not have a lot of Oxygen-excess galaxies dominated by star formation (i.e., those above the dashed line), but this is simply a selection bias that we cannot find weak AGNs in actively star forming galaxies because our method uses a contrast between L_{SF} and L_{AGN} . If [OII] was a perfect indicator of star formation, we would expect that galaxies line up at $L_{[OII],SF} / (L_{[OII],SF} + L_{[OII],AGN}) = 1$.

Starting with the left panel, [OII] due to AGN completely dominates in galaxies with low SFRs, while the star formation component comes in at moderate-high SFRs. This is a totally expected behavior. The observed [OII] does not give any sensible SFRs in quiescent galaxies. Even in actively star forming galaxies ($SFR_{\text{specfit}} \sim 1 M_{\odot} \text{ yr}^{-1}$), [OII] due to star formation does not dominate, although we are limited by the selection bias there.

One might expect that the AGN component becomes negligible in weak AGNs and [OII] might be a good indicator of SFRs. But, the middle plot in Fig. 9 shows that this is not the case. As we will discuss in the next section, there is a positive correlation between the AGN power and underlying star formation activities. Due to this correlation, there is no strong dependence between the dominance of SF/AGN component and AGN power. There is always a fair chance of suffering from AGN contribution in the observed [OII] luminosity.

Finally, the right panel shows the dominance of the star for-

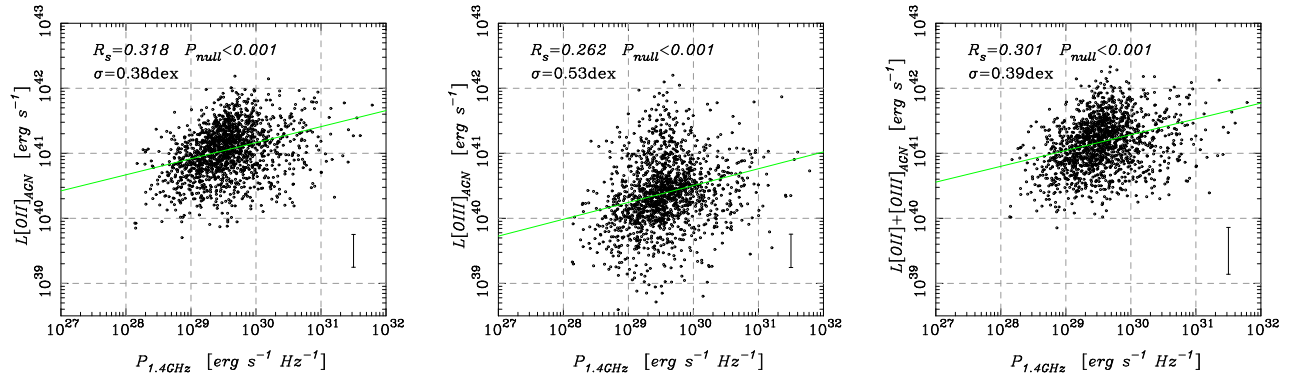


Fig. 8. As in Fig. 3, but here we compare optical emission line luminosities with radio power. FIRST sources dominated by star formation are removed from the plot. The median error is shown on the bottom-right corner. The integrated FIRST fluxes are measured by fitting elliptical Gaussian to the sources, which makes it difficult to evaluate the flux uncertainties (White et al. 1997). We do not quote the median uncertainty in the radio power.

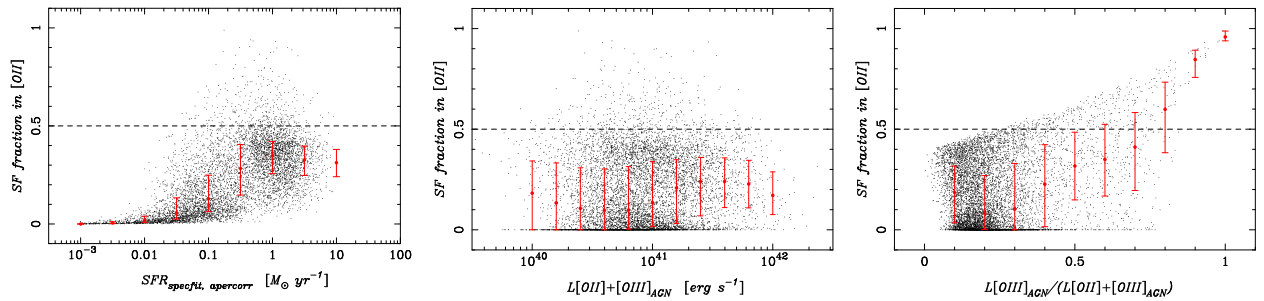


Fig. 9. *Left:* Fractional contribution of [OII] due to star formation to the overall [OII] luminosity plotted against SFR. The dashed line shows the equality of SFR and AGN components. Star formation dominates above the line and AGN dominates below the line. The points with error bars show the median and quartiles of the distribution. *Middle:* Same as the left panel, but here the horizontal axis is AGN power. *Right:* Same as the left panel, but the horizontal axis is ionization state. [OII]<[OIII] holds at [OIII]/([OII]+[OIII])>0.5, and [OII]>[OIII] holds at [OIII]/([OII]+[OIII])<0.5.

mation component as a function of ionization level. Most of the LINERs ($[OII]_{AGN} > [OIII]_{AGN}$) are dominated by AGN emission and [OII] due to star formation dominates only in the very high ionization galaxies. For the vast majority of low-luminosity AGNs, [OII] is unlikely a good indicator of star formation.

To be further quantitative, let us ask a simple question — if we assume that [OII] is entirely due to star formation, how well can we reproduce the SFRs of the hosts? Left panel in Fig. 10 gives the answer. We simply translate an observed [OII] luminosity into SFR using the formula given in Kennicutt (1998) without any subtraction of the AGN component or any dust correction. As can be seen, the SFRs from [OII] do not correlate with true SFRs very well. In particular, one grossly overestimates SFRs in quiescent galaxies. In those galaxies, star formation is very weak and the observed [OII] is nearly entirely due to AGN (Fig. 9 left panel). The assumption of [OII] due to star formation completely fails here. Another point to mention is that the systematic offset seen at $\sim 1 M_{\odot} \text{ yr}^{-1}$ is mostly due to the ignorance of dust. If we correct for $\tau_V = 1$ extinction, which is typical in star forming regions (Hopkins et al. 2003), the systematic offset is largely gone. However, the dust correction increases the discrepancy in low SFR galaxies because it shift all the points upwards.

As shown in Paper-I, the collisionally excited [OII] and [OIII] suffer (or benefit when we identify AGNs using these

lines) from AGN contribution, while $H\alpha$ is less affected. This is consistent with what the BPT diagram tells us — AGNs show stronger collisionally excited lines than the Balmer lines and that is why galaxies form a distinct sequence from the star formation sequence to the top-right corner of the diagram, not to the bottom-left corner. Due to the relatively weak AGN contribution to $H\alpha$, SFRs from $H\alpha$ indeed better agree with those from the spectral fits as shown in the right panel of Fig. 10. Therefore, $H\alpha$ is a better indicator of SFRs in AGNs than [OII]. However, $H\alpha$ still largely overestimates SFRs in quiescent galaxies by more than an order of magnitude.

To sum up, one should be cautious about using [OII] as an indicator of SFRs in AGNs. It can give SFRs that are offset by more than an order of magnitude. In particular, we suggest that one should not use [OII] when a host galaxy has red colors. The galaxy may be a dusty galaxy, but it may well be passive galaxies, for which [OII] is entirely due to AGN. As a result, one wildly overestimates SFRs. Also, dust extinction needs to be accounted for. One should use continuum information whenever available because the spectral fitting is likely to deliver better SFRs due to less AGN contamination to the continuum spectrum (Schmitt et al. 1999). It may often be the case when the continuum spectrum is not available with sufficient signal-to-noise ratios especially at high redshifts. Recent availability of multi-wavelength photometry would give a way around it. SED fits of multi-wavelength broad-band photome-

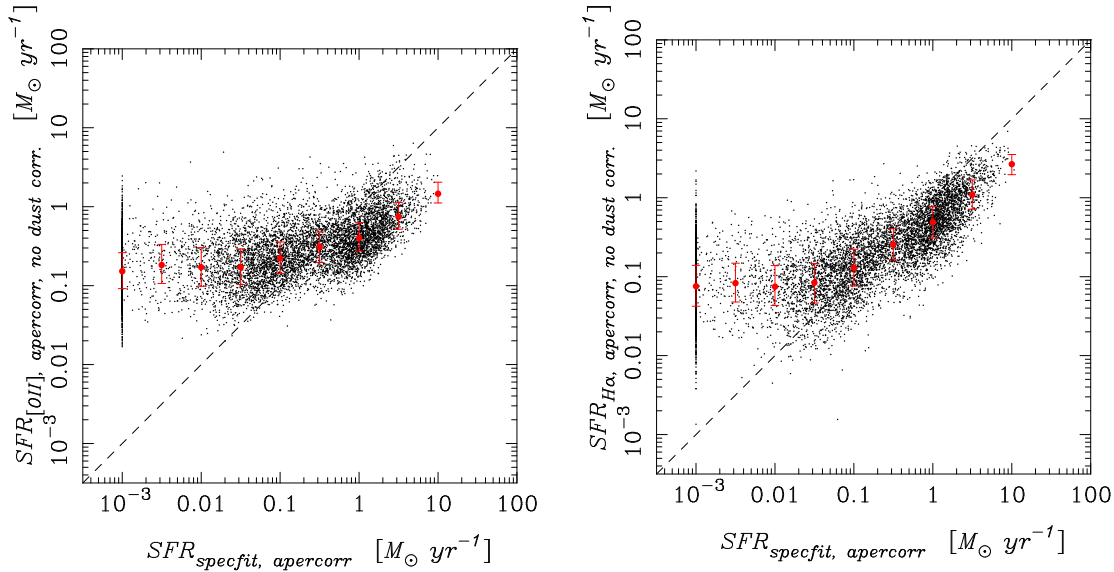


Fig. 10. SFRs from [OII] (left) and H α (right) plotted against SFRs from the spectral fits. We only correct for the fiber aperture loss and do not apply any further correction to [OII] and H α (i.e., no subtraction of AGN component and no correction for dust) and simply convert the observed luminosity into SFRs. The points with error bars show the median and quartiles of the distribution.

try seem to give reasonable SFR estimates (e.g., Santini et al. 2009). If one is careful enough to remove photometry that can be affected by AGN component (UV continuum or IR thermal emission) from the SED fits, it would provide better SFR estimates than [OII] and H α . We shall emphasize that the key is to use stellar light only. It would be challenging to estimate SFRs of QSOs, whose continuum is dominated by AGN emission, not by stars. If QSO continuum can be subtracted by assuming a power-law form, one can fit the spectrum of the remaining stellar component. An accuracy of SFRs from such a fit remains to be quantified.

4. Nature of the Oxygen-excess objects: AGN activities and the host galaxy properties

Following the development of the basis to characterize AGN activities, we now move on to discuss the nature of Oxygen-excess objects with an emphasis on the relationship between the AGN and host galaxy properties. We start with the fraction of AGNs as a function of host galaxy properties, followed by a detailed look at a partition between LINERs and Seyferts. We then show scatter plots of the host galaxy properties and black hole masses. Finally, we study the AGN activity and compare the black hole growth rate and the host galaxy growth rate.

4.1. Dependence of AGN fraction on Stellar mass, Color, SFR and Morphology

Essentially all galaxy properties depend on mass of galaxies and we start with stellar mass dependence of the AGN fraction in Fig. 11. The AGN fraction is a very strong function of stellar mass of host galaxies. Most AGNs that we have identified reside in galaxies with $M_{stellar, apercorr} > 10^{10} M_{\odot}$. In the most massive galaxies with $M_{stellar, apercorr} > 10^{11} M_{\odot}$, 60% of the galaxies harbor AGNs. We note that this is just a lower limit. A large fraction of galaxies in our sample do not exhibit

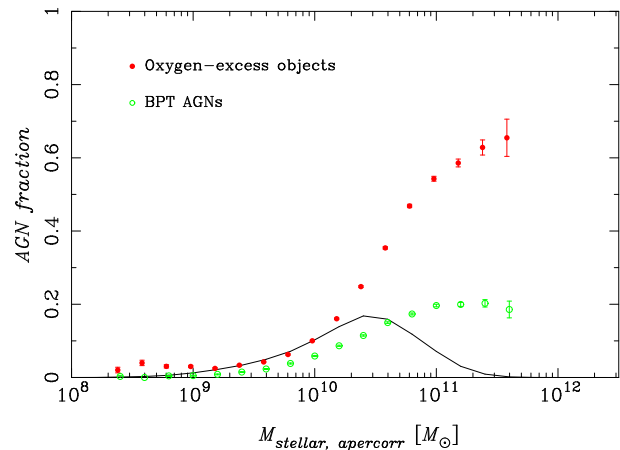


Fig. 11. Fraction of AGNs plotted against stellar mass. The filled and open circles are Oxygen-excess objects and AGNs from the BPT diagram, respectively. The solid line shows the fractional distribution of all the galaxies in our sample.

strong enough Oxygen lines to apply our method (i.e., OnBn defined in Paper-I) and the stacked spectrum of those galaxies exhibits LINER-like line ratios. Therefore, many of the unclassified galaxies may well be AGNs (see also discussions on the non-AGN photo-ionization in Paper-I and earlier sections of this paper). In contrast to the Oxygen-excess method, the BPT diagnostics gives an AGN fraction of only 20% in massive galaxies. This demonstrates the sensitivity of our method to identify AGNs.

Heckman et al. (2004) found that the fraction of active black holes (i.e., AGNs) is highest in intermediate mass black holes and it decreases in the most massive black holes based on BPT AGNs. We have replaced the stellar mass with black hole mass (see below for the derivation of the black hole mass) in Fig. 11

and found that a fraction of Oxygen-excess objects continues to increase towards the high mass end. This difference from Heckman et al. (2004) is due to the difference in the redshift ranges explored. Heckman et al. (2004) did not apply any redshift selection to the main galaxy sample (Strauss et al. 2002). Due to the flux limited nature of the sample, an average redshift of galaxies is higher for more massive galaxies and therefore an average sensitivity to emission line luminosity is lower. This resulted in a reduced sensitivity to identify AGNs in very massive galaxies and caused a decline in the fraction of active black holes at the high mass end. We have confirmed that we reproduce the Heckman et al. (2004)’s trend by changing the redshift range to $0 < z < 0.3$ and redoing the whole analysis.

We further discuss color, SFR and morphology dependence of the AGN fractions.

Color (Fig. 12): We compute rest-frame $u - r$ color from the model magnitudes (Stoughton et al. 2002) using the k -correction code by Blanton & Roweis (2007) and plot the AGN fraction as functions of stellar mass and rest-frame $u - r$ color. We find that Oxygen-excess objects prefer red galaxies ($u - r \gtrsim 2$) at all masses. As expected from the stellar mass dependence in Fig. 11, the fraction increases from low to high mass galaxies. The most massive galaxies show the highest AGN fraction, reaching to nearly 70%. The fraction decreases towards bluer colors, but this is at least partly driven by the selection bias that we cannot identify weak AGNs in actively star forming galaxies.

In contrast to the clear preference of Oxygen-excess objects to red colors, a large fraction of BPT AGNs reside in the green valley around $u - r \sim 2$ in consistent with Kauffmann et al. (2003) and Schawinski et al. (2010). This is due to the fact that BPT is not very sensitive to AGNs in passive galaxies. As shown later, most AGNs in passive galaxies are low-luminosity AGNs. They often show too weak $H\beta$ to apply the BPT method (see the stacked spectrum of O+Bn in Fig. 7 of Paper-I). As a result, the BPT misses a significant fraction of low-luminosity AGNs on the red sequence, and that causes the large difference in the AGN fraction in red galaxies between Oxygen-excess and BPT. In other words, BPT AGNs in the green valley are relatively strong AGNs. We note that objects detected in radio or X-ray do not show a clear excess in the green valley.

SFR (Fig. 13): In addition to the color, SFR is also one of the most important properties of galaxies. We quantify the AGN fraction as a function of SFRs and stellar mass of the host galaxies. Low-mass galaxies are predominantly star forming, but massive galaxies exhibit bimodal distribution of SFRs. The BPT AGN fraction shown in the right panel is constantly low at $\text{SFR} \lesssim 0.1 M_{\odot} \text{ yr}^{-1}$, but it shows a rapid increase at higher SFRs. On the other hand, the Oxygen-excess objects show a contrasting behavior. We interpret it by a combination of two effects. At low SFRs, the Oxygen-excess method is fairly sensitive and it gives a much higher AGN fraction than BPT. Because the method is based on identifying excess Oxygen luminosity, it becomes less efficient as underlying star formation becomes more active. This causes the drop of the AGN fraction around $1 M_{\odot} \text{ yr}^{-1}$, where significant star formation component kicks in (see Fig. 9). This plot shows the sensitivity function of

the Oxygen-excess method (we will further quantify it below). Its sensitivity is similar to BPT when SFRs are high, but it is much more sensitive at low SFRs. The Oxygen-excess method is suited to study AGNs in quiescent galaxies.

The fraction of Oxygen-excess objects seems to more strongly depend on stellar mass than on SFR. The fraction of Oxygen-excess objects with $\text{SFR} \sim 0.1 M_{\odot} \text{ yr}^{-1}$ drops from 70% at high mass to nearly 0% at low mass. Mass is likely the primary parameter to trigger the AGN activity.

Morphology (Fig. 14): As an indicator of morphology, we use the inverse concentration index (Shimasaku et al. 2001; Strateva et al. 2001) defined by R_{50}/R_{90} , where R_{50} and R_{90} are the radii which enclose 50% and 90% of the total light (Petrosian flux; Petrosian 1976; Stoughton et al. 2002) in the z -band to minimize effects of on-going star formation. The inverse concentration index is of course affected by the seeing. The median seeing in the z -band is 1.3 arcsec. We have confirmed that the trend in the plot does not change whether we use only objects observed under good seeing or not.

We quantify the AGN fraction as functions of the inverse concentration index and stellar mass in Fig. 14. Oxygen-excess objects tend to be massive early-type galaxies as expected from the color-stellar mass dependence discussed above. The Oxygen-excess fraction shows a mild dependence on morphology, but again, stellar mass seems to be the primary parameter to trigger AGN activity. It is interesting to note that even if galaxies exhibit early-type morphology, they do not show a hint of AGN activity at low mass. In contrast to Oxygen-excess objects, BPT AGNs prefer intermediate morphology as they are strongly biased towards green valley galaxies due to the poorly sampled low-luminosity AGNs.

Overall, Oxygen-excess objects tend to be massive red galaxies. The fraction of Oxygen-excess objects decreases towards blue, star-forming, late-type galaxies at a given stellar mass, but this is at least partly driven by the selection bias that we miss weak AGNs in actively star forming galaxies. On the other hand, the distribution of BPT AGNs is strongly skewed towards galaxies in the green valley. This is driven by the bias that BPT diagnostics is not very sensitive to low-luminosity AGNs on the red sequence. The figures presented in this section seem to suggest that BPT diagnostics does not provide an unbiased sample of AGNs. BPT AGNs are strongly biased. Oxygen-excess objects are also biased, but the selection bias is relatively straightforward to quantify as shown below because it is simply based on a contrast between AGN power and underlying star formation (it can be complicated when the featureless continuum emission from AGN significantly contributes to the overall spectra). We will carefully account for such biases in the following discussions.

4.2. Dependence of LINERs and Seyferts on host galaxies

Let us briefly mention the partition between LINERs and Seyferts among the Oxygen-excess objects as a function of host galaxy properties. We define LINERs as $[\text{OII}]_{\text{AGN}} > [\text{OIII}]_{\text{AGN}}$ as discussed in Section 3.2. We remind the readers again that the subscript *AGN* means that the luminosity due to star formation is subtracted and the ex-

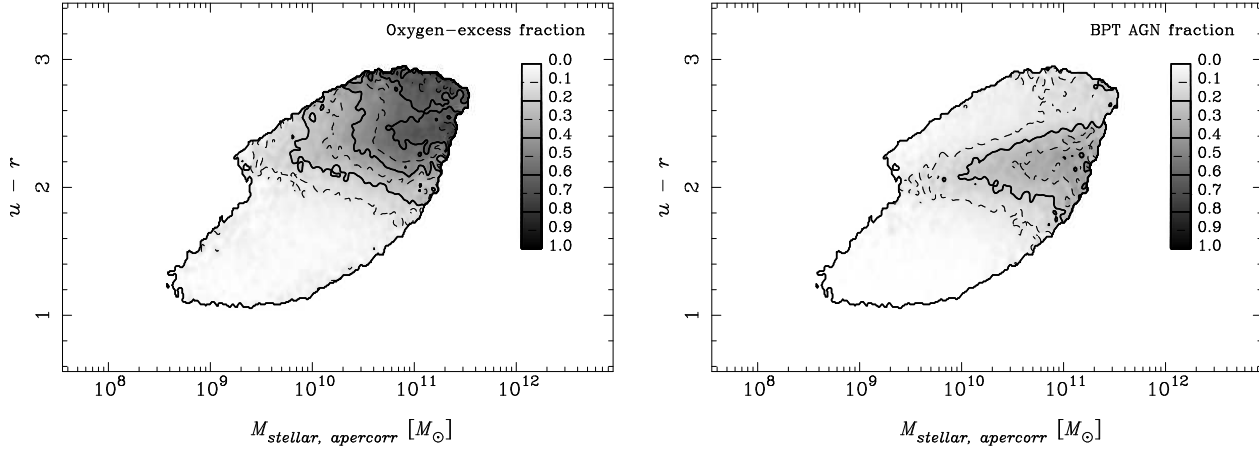


Fig. 12. **Left:** Fraction of Oxygen-excess objects as functions of rest-frame $u-r$ color and stellar mass. The solid contours show the fractions of 0, 20, 40, 60, 80, and 100%, and the dashed contours show 10, 30, 50, 70, and 90%. **Right:** As in the left panel, but here we show the fraction of BPT AGNs.

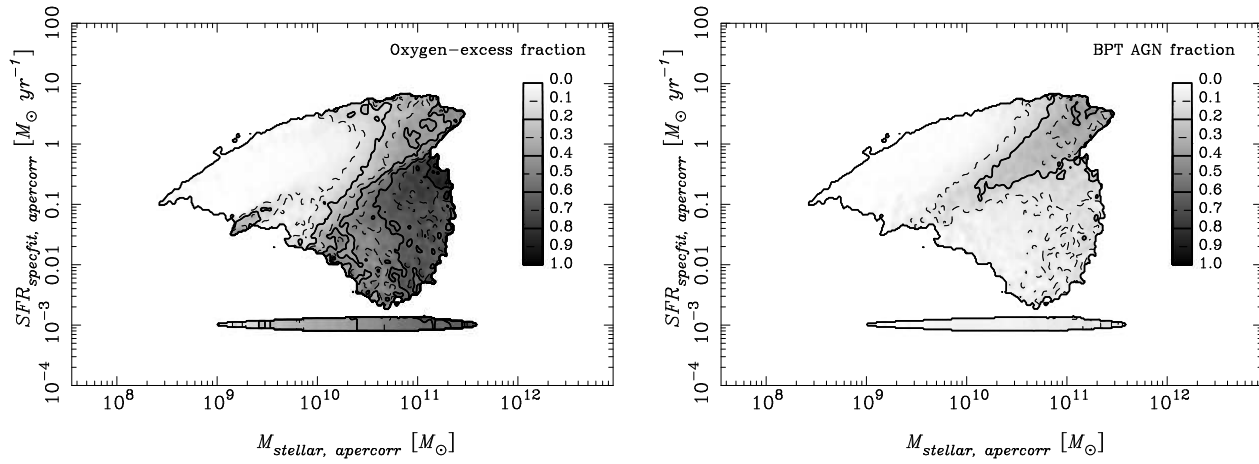


Fig. 13. **Left:** Fraction of Oxygen-excess objects as functions of SFR and stellar mass. The contours are the same as in Fig. 12. Galaxies with $SFR_s < 10^{-3} M_{\odot} \text{ yr}^{-1}$ are summed up at $SFR = 10^{-3} M_{\odot} \text{ yr}^{-1}$. **Right:** As in the left panel, but for BPT AGNs.

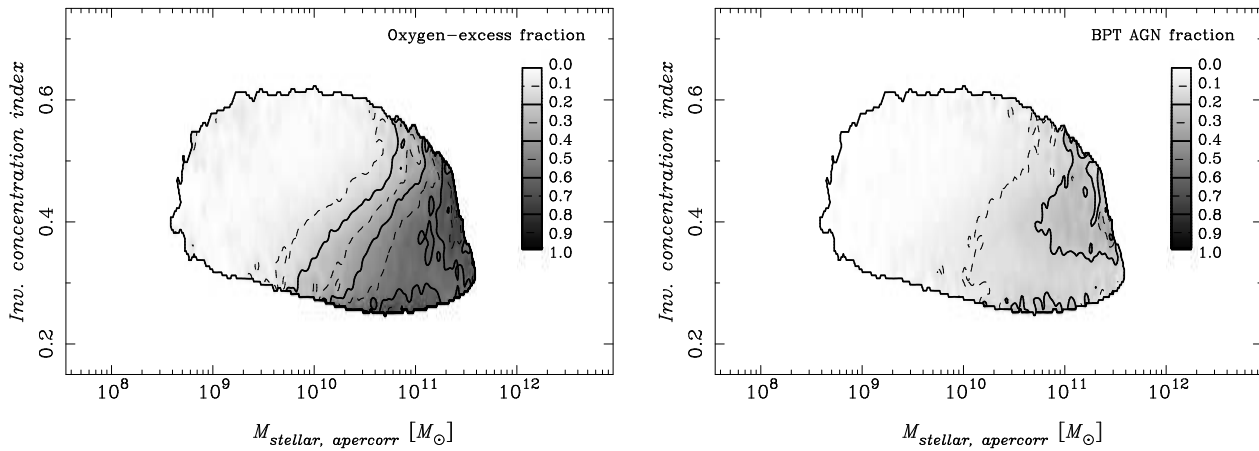


Fig. 14. **Left:** Fraction of Oxygen-excess objects as functions of inverse concentration index measured in the z -band and stellar mass. The contours are the same as in Fig. 12. **Right:** As in the left panel, but for BPT AGNs.

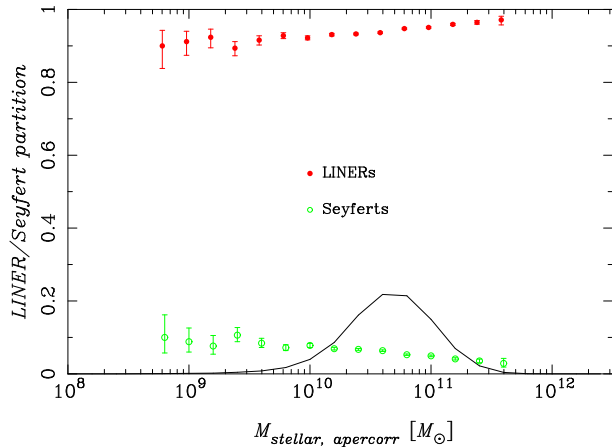


Fig. 15. Fractions of Seyferts and LINERs as a function of stellar mass. The filled and open circles show LINERs and Seyferts, respectively. The solid line shows the normalized distribution of all the Oxygen-excess galaxies.

tion correction described in Section 3.1 has been applied. Kewley et al. (2006) and Schawinski et al. (2007) studied the LINER/Seyfert partition using BPT AGNs, but we revisit the subject with pure AGN luminosities.

As in the last subsection, we start with stellar mass dependence shown in Fig. 15. It is striking that most Oxygen-excess objects are LINERs and the LINER/Seyfert partition shows only very weak dependence on stellar mass. This is in contrast to the strong stellar mass dependence of the AGN fraction discussed above. AGNs prefer massive galaxies, but once they become active, their activity (LINER vs Seyfert) does not strongly depend on mass. We will further discuss this ‘mass switch’ to activate AGNs in the next section.

Fig. 16 shows the LINER/Seyfert partition as functions of stellar mass, rest-frame $u - r$ color, SFR, morphology and AGN power. There is a weak trend that Seyferts increase in late-type, blue, star forming galaxies. Massive red, quiescent galaxies do not show Seyfert-like activities. This is qualitatively consistent with Kewley et al. (2006) who observed that typical age of stellar populations in Seyferts is younger than that of LINERs. It is also in agreement with Schawinski et al. (2007) that LINERs tend to be in quiescent galaxies. The LINER/Seyfert partition is apparently not strongly dependent on host galaxy properties, but we find that the partition is a relatively strong function of the AGN power. At $L_{[\text{OII}]+[\text{OIII}]_{\text{AGN}}} < 10^{41} \text{ erg s}^{-1}$, the Oxygen-excess objects are mostly LINERs. The Seyfert fraction rapidly increases towards high luminosity and Seyferts and LINERs almost equally exist in the most powerful objects studied here. We note that, within the redshift range explored ($0.02 < z < 0.1$), we are complete down to a luminosity of $L_{[\text{OII}]+[\text{OIII}]_{\text{AGN}}} = 3 \times 10^{40} \text{ erg s}^{-1}$ for quiescent galaxies. This number is derived from the lower boundary of galaxy distribution on a $L_{[\text{OII}]+[\text{OIII}]_{\text{AGN}}}$ vs redshift plot.

To summarize, the partition is primarily a function of AGN power and its dependence on host galaxy properties is relatively weak. Seyferts seem to slightly prefer star forming galaxies, but this correlation is likely due to a correlation be-

tween SFR and AGN power presented below.

4.3. Correlations between AGN activity and host galaxy properties

To further discuss the AGN activity, we introduce black hole mass. There are a few ways to estimate black hole mass. Here we take an empirical way and use the stellar velocity dispersion. Bulge stellar velocity dispersion is observed to exhibit a tight correlation with black hole masses (Gebhardt et al. 2000; Ferrarese & Merritt 2000; Tremaine et al. 2002; Gültekin et al. 2009). We use the velocity dispersion estimates from the MPA/JHU catalog (Tremonti et al. 2004; Kauffmann et al. 2004) and derive the black hole masses using the empirical relation from Tremaine et al. (2002):

$$\log(M_{\text{BH}}/M_{\odot}) = 8.13 + 4.02 \log(\sigma/200), \quad (6)$$

where σ is the stellar velocity dispersion in units of km s^{-1} . This calibration is consistent with a recent calibration (Gültekin et al. 2009). We should emphasize that our black hole mass estimates are nothing more than a rough guess and are only of a statistical value as warned by previous studies (e.g., Kauffmann et al. 2007). The SDSS measures the velocity dispersion within 3 arcsec fibers, and hence it is measured over different physical sizes for galaxies at different redshifts. A velocity component of disk will be a significant source of error in our black hole mass estimates. There is no straightforward way to correct for such an effect and dedicated observations would be needed for more accurate black hole mass estimates. Note that we remove objects with $\sigma < 70 \text{ km s}^{-1}$ from the catalog because of the limited SDSS spectral resolution of $R \sim 2000$.

We show in Fig. 17 correlations between the black hole mass and stellar mass, SFRs, morphology, and AGN power. Although not all the plots are entirely new and interesting, we show them as a representative set of correlations between the primary parameters. We make the following points from these plots.

Stellar mass: Black hole mass increases with increasing stellar mass. This correlation is expected given that more massive galaxies show higher stellar velocity dispersions. We obtain a Spearman’s rank correlation coefficient of 0.58 with a null probability of $\ll 10^{-5}$. Most Oxygen-excess objects have M_{BH} between 10^7 and $10^8 M_{\odot}$. This is similar to the black hole mass distribution of LINERs and Seyferts in the Palomar survey (Ho 2009).

SFR: Given the clear positive correlation between stellar mass and black hole mass, this plot is basically equivalent to a SFR vs stellar mass plot. Galaxies form two well-known sequences – star forming and quiescent. The bimodality is particularly clear in massive galaxies.

Morphology: Most of the Oxygen-excess objects exhibit early-type morphology with the inverse concentration index below 0.4 (Shimasaku et al. 2001; Strateva et al. 2001). The index gradually increases towards low black hole mass, but we are not sure if this is a real trend. Lower mass objects appear smaller on the sky and thus they are more strongly affected by the seeing effect, which results in in-

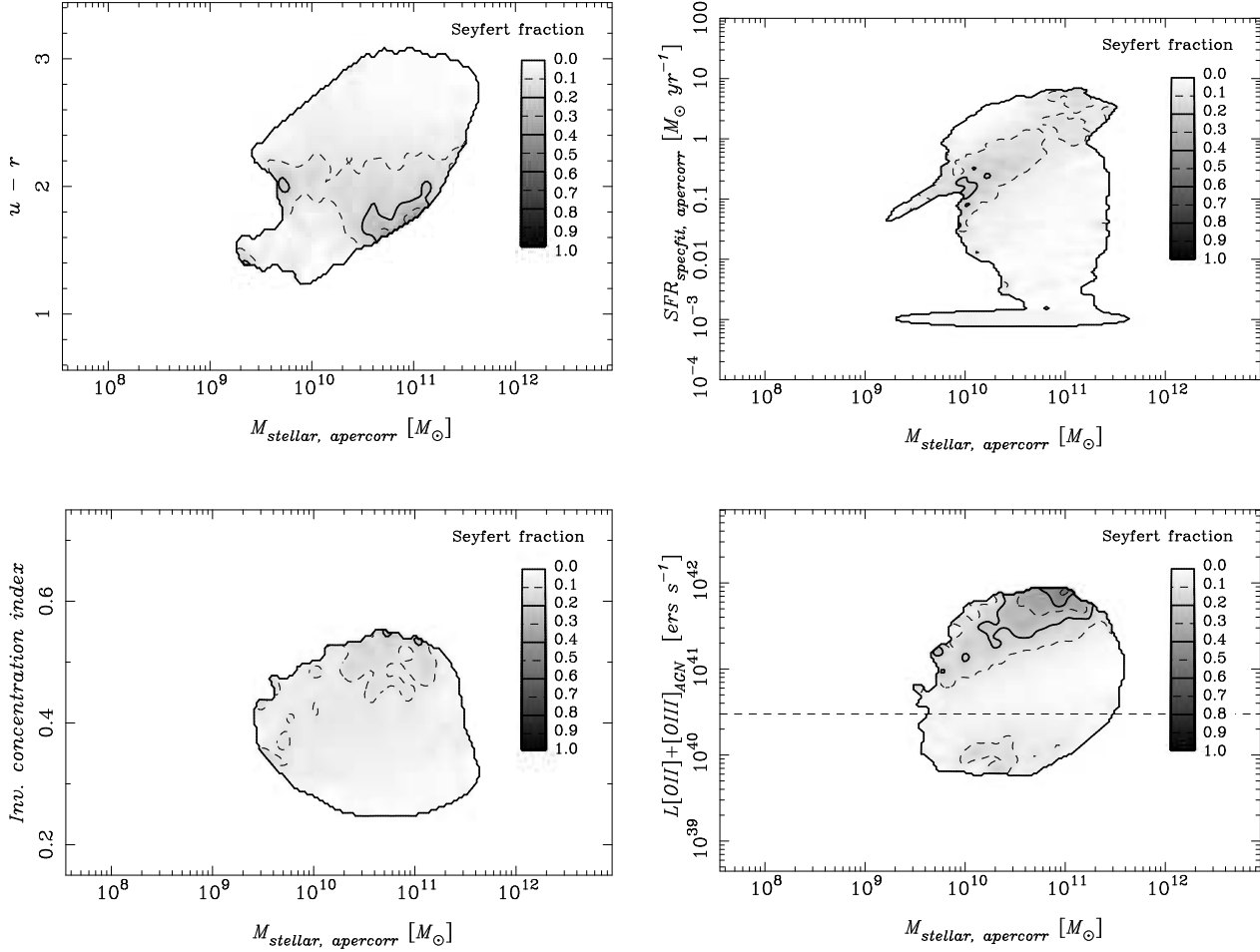


Fig. 16. Fraction of Seyfert galaxies ($[\text{OII}]_{\text{AGN}} < [\text{OIII}]_{\text{AGN}}$) among all the Oxygen-excess objects. The panels show the fraction as functions of stellar mass and rest-frame $u - r$ color (top-left), SFR (top-right), inverse concentration index (bottom-left), and AGN power (bottom-right). We show our sensitivity limit of AGN power in the bottom-right panel as the dashed line. The contours are as in Fig. 12.

creased inverse concentration index. But, in any case, it is fair to say that most Oxygen-excess objects are early-type galaxies.

AGN power: There seems to be a weak positive correlation between the AGN power and black hole mass, although the scatter is very large. A Spearman’s correlation coefficient is 0.10, but the null hypothesis is rejected with a $\ll 10^{-5}$ probability. Such a weak correlation is surprising given the strong stellar mass dependence of the AGN fraction discussed in Section 4.1. We recall that we did not observe a clear correlation between hard X-ray luminosity and stellar mass in Fig. 5. A similar trend has been observed by other authors (Aird et al. 2011; Mullaney et al. 2012). We will elaborate on the trend in Section 5.

4.4. The co-evolution of black holes and host galaxies

We have quantified the basic correlations between the primary parameters and we now characterize relationships between activities and growth rates of AGNs and those of host galaxies. Fig. 18 shows the correlation between AGN power

and host galaxy SFR. This plot therefore compares the activities of the host galaxies in terms of star formation (\dot{M}_{stellar}) and the accretion rate of the central black hole (\dot{M}_{BH}). We recall that we have subtracted the star formation component from the $[\text{OII}]+[\text{OIII}]$ luminosity and corrected for extinction, thereby representing intrinsic AGN emission. The slanted dashed lines are our selection bias mentioned several times by now. Because we require a significant L_{AGN} with respect to L_{SF} in Eq. 1, we miss weak AGNs in actively star forming galaxies. The dashed lines are the limits where L_{AGN} can be detected at 1.5σ ($> 1.5\sigma$ is the definition of Oxygen-excess) at a given L_{SF} for galaxies with typical extinction. Unlike BPT, the selection bias of the Oxygen-excess method is understood fairly well.

The AGN power seems to increase with increasing SFRs. But, the trend is driven by the incompleteness at the bottom-right corner of the plots due to the selection bias. The plot does not give us an average AGN power as a function of SFR, and we can only discuss the upper envelope of the AGN power distribution. AGNs in low-SFR galaxies are typically of low-luminosity and few powerful AGNs (several times 10^{41} erg s^{-1} , say) are located in those galaxies. The upper

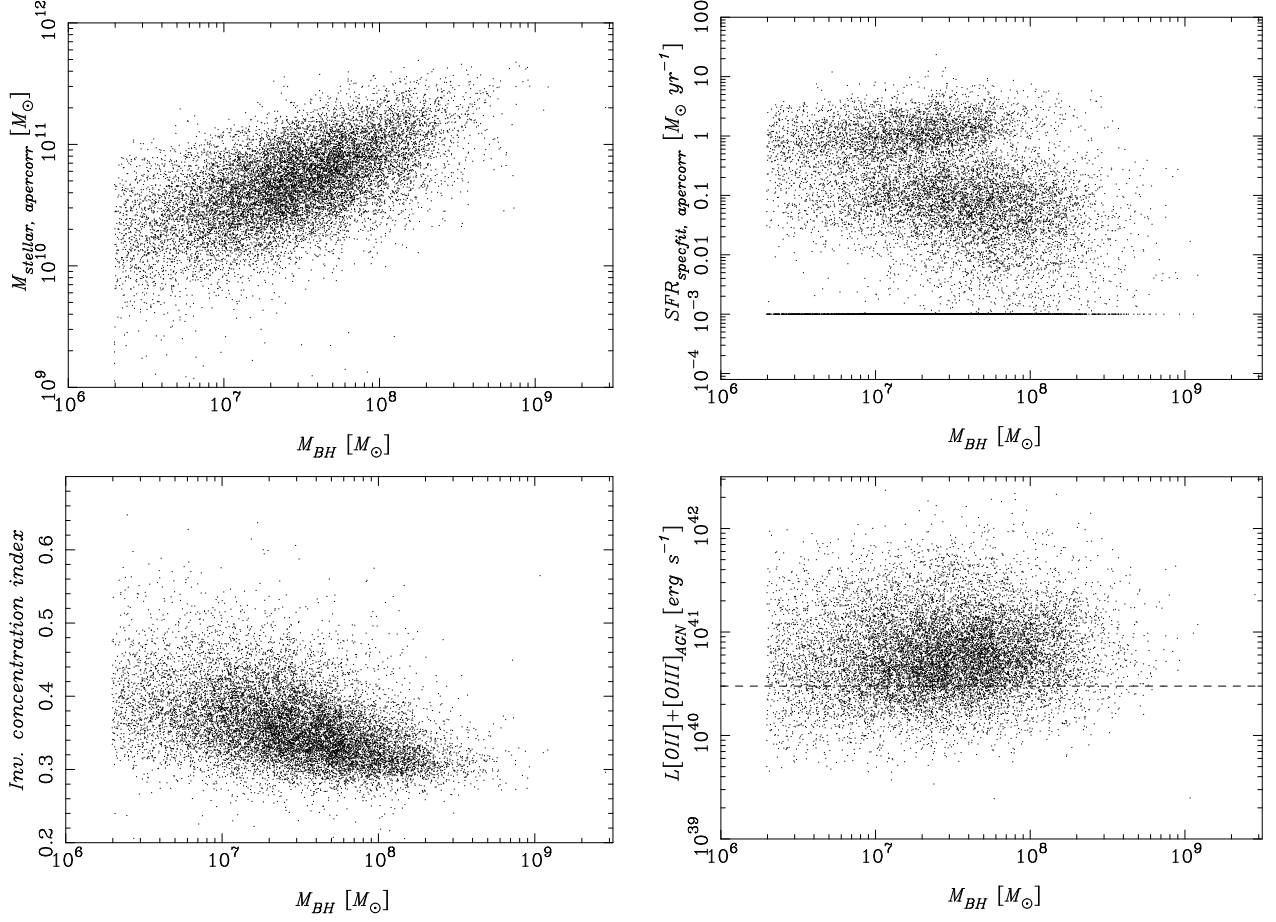


Fig. 17. Correlations between M_{BH} and stellar mass (top-left), SFR (top-right), inverse concentration index (bottom-left), and AGN power (bottom-right).

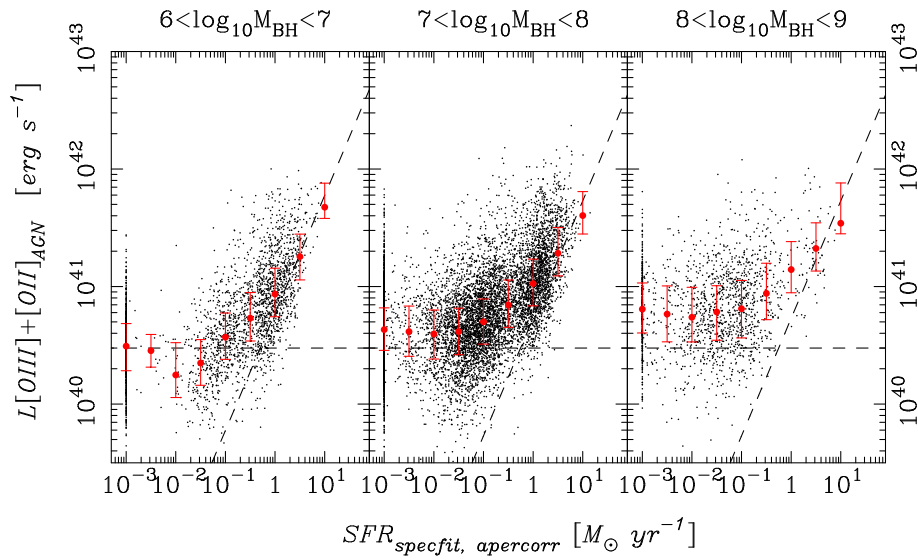


Fig. 18. AGN power plotted against redshift. The dots are Oxygen-excess objects and the large point with the error bar shows the median and quartile of $L[OII] + [OIII]_{AGN}$ of galaxies in each SFR bin. The horizontal dashed lines show detection limits and the slanted dashed lines are the selection function. We miss weak AGNs in actively star forming galaxies.

envelope of the AGN power distribution extends to higher luminosity at higher SFRs and powerful AGNs are often hosted by actively star forming galaxies. This suggests that galaxies and the central black holes can become active simultaneously. This is a surprising phenomenon because galaxy star formation and the central AGN activity occur on a very different physical scales (10 kpc vs. 1 pc).

The AGN power is on average lowest at $\text{SFR} < 0.1 M_{\odot} \text{ yr}^{-1}$. This weak AGN power in quiescent galaxies is again the point we have often mentioned above. Weak AGNs tend to reside in quiescent galaxies in our sample. In other words, AGNs on the red sequence are low-luminosity AGNs. These are the galaxies that BPT tends to miss; as we have shown in Fig. 12, the BPT gives a low AGN rate on the red sequence, while we find a large AGN population there. On the other hand, strong AGNs are located in actively star forming galaxies and we find that they tend to fill in the green valley in line with previous studies (Schawinski et al. 2007; Schawinski et al. 2010).

The AGN power - SFR relation observed in Fig. 18 may provide a physical link between the down-sizing in galaxy star formation (e.g., Thomas et al. 2005) and the down-sizing in AGN activities (Ueda et al. 2003). More massive galaxies form at earlier times with shorter star formation time scales. The peak SFRs of galaxies are therefore higher for more massive galaxies. Fig 10 of Thomas et al. (2005) qualitatively illustrates it. If the AGN power is correlated with the SFRs as shown in Fig. 18 at all redshifts, then we expect to observe a peak of space density of stronger AGNs at higher redshifts. Ueda et al. (2003) actually observed that a peak of stronger AGN activity is located at higher redshifts. Perhaps the two down-sizing phenomena are linked by the co-evolution of black holes and host galaxies.

To obtain deeper insights into the relationship between the AGNs and host galaxies, we compare black hole growth rate ($L_{[\text{OII}]+[\text{OIII}]_{\text{AGN}}}/M_{\text{BH}}$, which is proportional to $\dot{M}_{\text{BH}}/M_{\text{BH}}$), and host galaxy growth rate ($\text{SFR}/M_{\text{stellar}}$, which is $\dot{M}_{\text{stellar}}/M_{\text{stellar}}$) in Fig. 19. $L_{[\text{OII}]+[\text{OIII}]_{\text{AGN}}}/M_{\text{BH}}$ also serves as an indicator of the Eddington ratio. We observe a tight correlation between $H\alpha$ and $[\text{OII}]+[\text{OIII}]$ ($L_{[\text{OII}]+[\text{OIII}]_{\text{AGN}}} \sim 4.5L_{H\alpha_{\text{AGN}}}$) and we obtain a bolometric correction factor of 50 to $L_{[\text{OII}]+[\text{OIII}]_{\text{AGN}}}$ assuming $L_{\text{bol}} \sim 220L_{H\alpha}$ from Ho (2008). We find that most of the Oxygen-excess objects typically have an Eddington ratio between 10^{-4} and 10^{-2} . We note that a bolometric correction to convert an emission line luminosity into bolometric luminosity is highly uncertain and probably not a constant correction (Ho 2008). Therefore, the Eddington ratio should not be over-interpreted.

We are again limited by the sensitivity limit and selection bias, but galaxies with lower mass black holes (i.e., lower mass galaxies) tend to show higher black hole growth rates and galaxy growth rates. In any black hole mass bin, the black hole growth rate is low at low $\text{SFR}/M_{\text{stellar}}$ and few objects with high $L_{[\text{OII}]+[\text{OIII}]}/M_{\text{BH}}$ are observed. The upper envelope of the black hole growth rate increases with increasing host galaxy growth rate and rapidly growing black holes are always hosted by rapidly growing galaxies. This clearly represents the co-evolution of the super-massive black holes and their host

galaxies. Again, this is surprising because these two growths occur at very different physical scales. The black hole growth occurs on a 1 pc scale (or less), while the galaxy growth occurs on a 10 kpc scale. But, our result shows that black holes grow in growing galaxies.

There are many recent speculations on energy feedback from AGNs to suppress star formation activities of the host galaxies. Do we observe any hint of AGN feedback in action in our data? The positive correlation in the upper envelope of the AGN power and host galaxy SFR suggests that strong AGNs do not appear to suppress on-going star formation. If strong AGNs could sharply suppress star formation, we would not have observed the positive correlation between AGN power and host galaxy SFRs. However, there may be a time delay between AGN activities and the suppression of SFRs. Also, the apparent lack of suppressed SFRs may possibly be because we do not probe very strong AGNs such as QSOs, in which star formation may be suppressed (Ho 2005; Kim et al. 2006).

On the other hand, the observed large fraction of AGNs in quiescent galaxies may give a support to the so-called 'radio mode' feedback (Croton et al. 2006; Bower et al. 2006), which suppresses gas cooling for further star formation and keeps red galaxies red. Our data, however, do not tell us whether these AGNs are actually suppressing the gas cooling and they have any direct effect on the host galaxies. We cannot make anything more than a speculation here, and it would be fair to say that we do not observe any convincing evidence of AGN feedback in action and we do not observe any evidence against it.

Some of the results in this subsection are already mentioned in previous studies using colors as a proxy for star formation rate. But, we have characterized them with physical parameters such as host galaxy SFRs. We shall also emphasize again that we have studied intrinsic AGN emission thanks to the unique feature of the Oxygen-excess method taking into account the selection bias. We have put the previous results on the quantitative ground and it is now clear that growing black holes are often hosted by growing galaxies, which represents the co-evolution of black holes and the host galaxies.

5. Summary and Discussion

In the last section, we have studied correlations between host galaxy properties and AGN activities. Among the numerous plots presented there, our primary findings can be summarized as follows.

1. The AGN fraction increases with increasing stellar mass of the host galaxies. Most of the AGNs are located in $> 10^{10} M_{\odot}$ galaxies.
2. The AGN fraction is higher in red early-type galaxies than in blue late-type galaxies. But, this is at least partly driven by the fact that the Oxygen-excess method tends to miss low-luminosity AGNs in actively star forming galaxies.
3. Most of the identified AGNs are LINERs. The LINER/Seyfert partition is primarily a function of AGN power and its dependence on host galaxy properties is weak. Seyfert-like AGNs with $[\text{OII}]_{\text{AGN}} < [\text{OIII}]_{\text{AGN}}$ appear only in powerful AGNs.

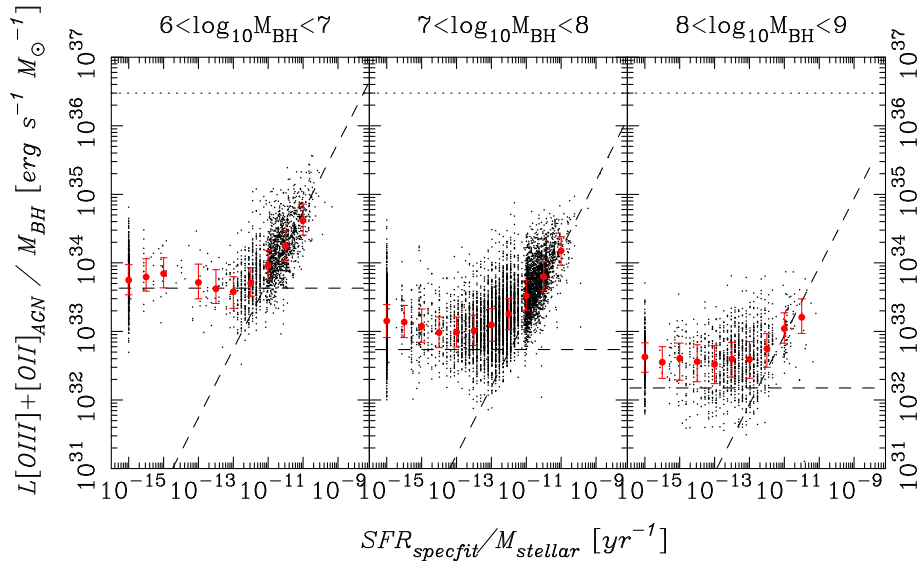


Fig. 19. $L_{[OII]+[OIII]_{AGN}}/M_{BH}$ plotted against $SFR/M_{stellar}$. The dashed lines are our detection limit and selection function. The dotted line is an approximate Eddington limit. The galaxies are distributed in vertical stripes due to the discrete model grids.

4. AGN power does not strongly correlate with black hole mass (or stellar mass of the host).
5. Powerful AGNs are located in actively star forming galaxies.
6. Rapidly growing black holes are hosted by rapidly growing galaxies.
7. We observe no direct evidence of the AGN feedback in action.

We find the 1st and 4th points above very interesting. The first point is shown in Fig. 11 and the 4th point is in Fig. 5 and the bottom-right panel of Fig. 17. Mass is the primary parameter to characterize the fraction of AGNs. The AGN fraction is very small below $10^{10} M_{\odot}$, but it increases rapidly above that mass. One might suspect that the lower AGN fraction at lower mass is because lower mass black holes show weaker activities and they go undetected. However, the 4th point above suggests that is not the case. The correlation between AGN power and mass is very weak and it is unlikely that such a weak correlation can explain the observed strong mass dependence of the AGN fraction. Recently, Mullaney et al. (2012) reached the same conclusion. Furthermore, lower-mass galaxies are located at lower redshifts due to the nature of a flux limited survey. The detection limit on $L_{[OII]+[OIII]_{AGN}}$ shown by the dashed lines in the figures is a limit at which we can detect it at all redshift ($0.02 < z < 0.10$) and our sensitivity is actually better for low-mass galaxies which we can observe only at low redshifts. The observed lack of low-mass AGNs is not due to the absence of bulge either. As shown in Fig. 14, the AGN fraction is very low at low mass regardless of the morphology. While very low-mass AGNs do exist (e.g., NGC4395 has $M_{BH} \sim 4 \times 10^5 M_{\odot}$; Peterson et al. 2005; see also the work by Barth et al. 2008), the observed strong mass dependence suggests that such low-mass AGNs are rare. It seems that mass is like a 'switch' to activate super-massive black holes.

There are at least two very naive interpretations of this absence of low-mass AGNs. One is that super-massive black

holes exist in all galaxies, but low-mass galaxies cannot transport material to the center and feed super-massive black holes for some reason. That is, the majority of the black holes are inactive and thus are not detected. In this scenario, a process to trigger AGN activity is unlikely related to the presence of bulge because the AGN fraction is nearly zero in low-mass galaxies regardless of their morphology (Fig. 14). Also, the presence/lack of a transportation mechanism must be largely independent of the accretion rate as we observed no strong correlation between the AGN power and black hole mass (Figs. 5 and 17). Namely, a mass transportation mechanism is established at a higher rate in more massive galaxies, but the transportation rate should be largely independent of mass. Although such a physical process is somewhat difficult to imagine, this is a possible interpretation of the result.

The other very naive interpretation is that the majority of low-mass galaxies do not host super-massive black holes. This is perhaps an extreme idea, but it does explain the observed trend because the presence/absence of super-massive black holes works just like a switch. If a galaxy hosts a super-massive black hole, it can be active if the host can feed it. If a galaxy does not harbor a super-massive black hole, it can never be active regardless of the host galaxy properties. In this scenario, mass of the host galaxies is a probability function of the presence of super-massive black holes. The form of the probability function is such that more massive galaxies are more likely to host super-massive black holes and the probability is very small at $< 10^{10} M_{\odot}$. In fact, the super-massive black hole occupation fraction is apparently small in low-mass galaxies (e.g., M33 and NGC205 do not host a super-massive black hole; Gebhardt et al. 2001; Valluri et al. 2005). This provides supportive evidence of the decreasing probability of hosting super-massive black holes with decreasing the host galaxy mass.

Mullaney et al. (2012) observed that the AGN activity is nearly independent of host galaxy stellar mass at $0 < z < 3$. They also observed that AGNs are almost exclusively hosted

by $> 10^{10} M_{\odot}$ galaxies. It seems that the trends that we observe at $z = 0$ holds out to $z = 3$. This might suggest that a primary epoch of the formation of super-massive black holes is located at very high redshift. Dark matter halos that collapse at high redshifts are among the most massive ones today and therefore the dominance of AGNs in massive galaxies is naturally explained if the formation of super-massive black holes peaked at high redshifts. The absence of low-mass AGNs might in turn imply that the super-massive black hole formation is not very efficient at low redshift. Perhaps the mass dependence of the AGN fraction reflects the formation history of the super-massive black holes.

Our data do not allow us to conclude which of the two scenarios discussed above is more likely. Also, there may well be other ways to interpret our result. Before we try to make any further speculations, we have to make an attempt to confirm that an AGN fraction in low-mass galaxies is actually very low compared to that in high-mass galaxies. An SDSS fiber subtends 3 arcsec on the sky, which corresponds to ~ 3 kpc at $z = 0.05$. AGN emission, if any, is therefore strongly contaminated by host galaxies. Also, our black hole mass estimates are probably not very accurate. Greene & Ho (2007) argued that the black hole mass function decreases at low mass. Our result may not be directly comparable to theirs because their result is based on objects with broad $H\alpha$ emission, while ours is based on narrow line AGNs. But, the observed decline in the black hole mass function at low-mass end is qualitatively consistent with ours. Still, it would be necessarily to carry out a dedicated observation to sample the nuclear spectra of nearby low-mass galaxies to achieve a better sensitivity to identify AGNs. If the absence of AGNs in low-mass galaxies is confirmed in such a survey, then we will be in a position to further discuss the physical origin of such a trend.

We thank John Silverman for extensive discussions, Luis Ho, and Yoshihiro Ueda for useful conversations, Yen-Ting Lin for helpful comments, and Naoki Yasuda for providing the computing environment. This work was supported by World Premier International Research Center Initiative (WPI Initiative), MEXT, Japan and also in part by KAKENHI No. 23740144. This research has made use of data obtained from the Chandra Source Catalog, provided by the Chandra X-ray Center (CXC) as part of the Chandra Data Archive. We thank the anonymous referee for his/her useful comments, which helped improve the paper.

Funding for the Sloan Digital Sky Survey (SDSS) and SDSS-II has been provided by the Alfred P. Sloan Foundation, the Participating Institutions, the National Science Foundation, the U.S. Department of Energy, the National Aeronautics and Space Administration, the Japanese Monbukagakusho, and the Max Planck Society, and the Higher Education Funding Council for England. The SDSS Web site is <http://www.sdss.org/>.

The SDSS is managed by the Astrophysical Research Consortium (ARC) for the Participating Institutions. The Participating Institutions are the American Museum of Natural History, Astrophysical Institute Potsdam, University of Basel, University of Cambridge, Case Western Reserve University,

The University of Chicago, Drexel University, Fermilab, the Institute for Advanced Study, the Japan Participation Group, The Johns Hopkins University, the Joint Institute for Nuclear Astrophysics, the Kavli Institute for Particle Astrophysics and Cosmology, the Korean Scientist Group, the Chinese Academy of Sciences (LAMOST), Los Alamos National Laboratory, the Max-Planck-Institute for Astronomy (MPIA), the Max-Planck-Institute for Astrophysics (MPA), New Mexico State University, Ohio State University, University of Pittsburgh, University of Portsmouth, Princeton University, the United States Naval Observatory, and the University of Washington.

References

- Abazajian, K. N., et al. 2009, *ApJS*, 182, 543
Aird, J., Coil, A. L., Moustakas, J., et al. 2011, arXiv:1107.4368
Baldwin, J. A., Phillips, M. M., & Terlevich, R. 1981, *PASP*, 93, 5
Barth, A. J., Greene, J. E., & Ho, L. C. 2008, *AJ*, 136, 1179
Baum, S. A., & Heckman, T. 1989, *ApJ*, 336, 702
Becker, R. H., White, R. L., & Helfand, D. J. 1995, *ApJ*, 450, 559
Binette, L., Magris, C. G., Stasińska, G., & Bruzual, A. G. 1994, *A&A*, 292, 13
Blanton, M. R., & Roweis, S. 2007, *AJ*, 133, 734
Bower, R. G., Benson, A. J., Malbon, R., Helly, J. C., Frenk, C. S., Baugh, C. M., Cole, S., & Lacey, C. G. 2006, *MNRAS*, 370, 645
Bruzual, G., & Charlot, S. 2003, *MNRAS*, 344, 1000
Cardelli, J. A., Clayton, G. C., & Mathis, J. S. 1989, *ApJ*, 345, 245
Charlot, S., & Fall, S. M. 2000, *ApJ*, 539, 718
Cid Fernandes, R., Stasińska, G., Mateus, A., & Vale Asari, N. 2011, *MNRAS*, 249
Colless, M., et al. 2003, arXiv:astro-ph/0306581
Cox, D. P. 1972, *ApJ*, 178, 143
Croton, D. J., et al. 2006, *MNRAS*, 365, 11
Dahari, O., & De Robertis, M. M. 1988, *ApJ*, 331, 727
de Gasperin, F., Merloni, A., Sell, P., et al. 2011, *MNRAS*, 415, 2910
Dickey, J. M., & Lockman, F. J. 1990, *ARA&A*, 28, 215
Doi, M., et al. 2010, *AJ*, 139, 1628
Dopita, M. A., & Sutherland, R. S. 1995, *ApJ*, 455, 468
Dopita, M. A., & Sutherland, R. S. 1996, *ApJS*, 102, 161
Eisenstein, D. J., et al. 2001, *AJ*, 122, 2267
Eracleous, M., Hwang, J. A., & Flohic, H. M. L. G. 2010, *ApJ*, 711, 796
Evans, I. N., et al. 2010, *ApJS*, 189, 37
Ferrarese, L., & Merritt, D. 2000, *ApJL*, 539, L9
Ferland, G. J., & Netzer, H. 1983, *ApJ*, 264, 105
Fukugita, M., Ichikawa, T., Gunn, J. E., Doi, M., Shimasaku, K., & Schneider, D. P. 1996, *AJ*, 111, 1748
Gaskell, C. M., & Ferland, G. J. 1984, *PASP*, 96, 393
Gebhardt, K., et al. 2000, *ApJL*, 539, L13
Gebhardt, K., et al. 2001, *AJ*, 122, 2469
Granato, G. L., De Zotti, G., Silva, L., Bressan, A., & Danese, L. 2004, *ApJ*, 600, 580
Greene, J. E., & Ho, L. C. 2005, *ApJ*, 630, 122
Greene, J. E., & Ho, L. C. 2007, *ApJ*, 667, 131
Greene, J. E., Zakamska, N. L., Ho, L. C., & Barth, A. J. 2011, *ApJ*, 732, 9
Gültekin, K., Cackett, E. M., Miller, J. M., Di Matteo, T., Markoff, S., & Richstone, D. O. 2009, *ApJ*, 706, 404
Gunn, J. E., et al. 1998, *AJ*, 116, 3040
Gunn, J. E., et al. 2006, *AJ*, 131, 2332
Halpern, J. P., & Steiner, J. E. 1983, *ApJL*, 269, L37
Heckman, T. M. 1980, *A&A*, 87, 152

- Heckman, T. M., Kauffmann, G., Brinchmann, J., Charlot, S., Tremonti, C., & White, S. D. M. 2004, *ApJ*, 613, 109
- Heckman, T. M., Ptak, A., Hornschemeier, A., & Kauffmann, G. 2005, *ApJ*, 634, 161
- Hes, R., Barthel, P. D., & Fosbury, R. A. E. 1993, *Nature*, 362, 326
- Ho, L. C., Filippenko, A. V., & Sargent, W. L. W. 1993, *ApJ*, 417, 63
- Ho, L. C., Filippenko, A. V., & Sargent, W. L. W. 1995, *ApJS*, 98, 477
- Ho, L. C., Filippenko, A. V., & Sargent, W. L. W. 1997, *ApJS*, 112, 315
- Ho, L. C. 1999, *ApJ*, 510, 631
- Ho, L. C. 2005, *ApJ*, 629, 680
- Ho, L. C. 2008, *ARA&A*, 46, 475
- Ho, L. C. 2009, *ApJ*, 699, 626
- Hopkins, A. M., et al. 2003, *ApJ*, 599, 971
- Juneau, S., Dickinson, M., Alexander, D. M., & Salim, S., 2011, arXiv:1105.3194
- Kauffmann, G., et al. 2003, *MNRAS*, 346, 1055
- Kauffmann, G., White, S. D. M., Heckman, T. M., Ménard, B., Brinchmann, J., Charlot, S., Tremonti, C., & Brinkmann, J. 2004, *MNRAS*, 353, 713
- Kauffmann, G., et al. 2007, *ApJS*, 173, 357
- Kennicutt, R. C., Jr. 1998, *ARA&A*, 36, 189
- Kewley, L. J., Dopita, M. A., Sutherland, R. S., Heisler, C. A., & Trevena, J. 2001, *ApJ*, 556, 121
- Kewley, L. J., Groves, B., Kauffmann, G., & Heckman, T. 2006, *MNRAS*, 372, 961
- Kim, D.-W., & Fabbiano, G. 2004, *ApJ*, 611, 846
- Kim, M., Ho, L. C., & Im, M. 2006, *ApJ*, 642, 702
- Kormendy, J., & Richstone, D. 1995, *ARA&A*, 33, 581
- Lamareille, F., Mouhcine, M., Contini, T., Lewis, I., & Maddox, S. 2004, *MNRAS*, 350, 396
- Lin, Y.-T., Shen, Y., Strauss, M. A., Richards, G. T., & Lunnan, R. 2010, *ApJ*, 723, 1119
- Lynden-Bell, D. 1969, *Nature*, 223, 690
- Magorrian, J., et al. 1998, *AJ*, 115, 2285
- Mainieri, V., Hasinger, G., Cappelluti, N., et al. 2007, *ApJS*, 172, 368
- Maoz, D., Koratkar, A., Shields, J. C., Ho, L. C., Filippenko, A. V., & Sternberg, A. 1998, *AJ*, 116, 55
- Morrison, R., & McCammon, D. 1983, *ApJ*, 270, 119
- Mullaney, J. R., Pannella, M., Daddi, E., et al. 2012, *MNRAS*, 419, 95
- Osterbrock, D. E. 1977, *ApJ*, 215, 733
- Osterbrock, D. E., & Ferland, G. J., 2006, *Astrophysics of Gaseous Nebulae and Active Galactic Nuclei*, Second Edition, University Science Books
- Pagel, B. E. J., Edmunds, M. G., Blackwell, D. E., Chun, M. S., & Smith, G. 1979, *MNRAS*, 189, 95
- Peterson, B. M., et al. 2005, *ApJ*, 632, 799
- Petrosian, V. 1976, *ApJL*, 209, L1
- Rawlings, S., & Saunders, R. 1991, *Nature*, 349, 138
- Richards, G. T., et al. 2002, *AJ*, 123, 2945
- Rola, C. S., Terlevich, E., & Terlevich, R. J. 1997, *MNRAS*, 289, 419
- Santini, P., et al. 2009, *A&A*, 504, 751
- Sarzi, M., Shields, J. C., Schawinski, K., et al. 2010, *MNRAS*, 402, 2187
- Saunders, R., Baldwin, J. E., Rawlings, S., Warner, P. J., & Miller, L. 1989, *MNRAS*, 238, 777
- Schawinski, K., Thomas, D., Sarzi, M., Maraston, C., Kaviraj, S., Joo, S.-J., Yi, S. K., & Silk, J. 2007, *MNRAS*, 382, 1415
- Schawinski, K., et al. 2010, *ApJ*, 711, 284
- Schmitt, H. R., Storchi-Bergmann, T., & Cid Fernandes, R. 1999, *MNRAS*, 303, 173
- Shimasaku, K., et al. 2001, *AJ*, 122, 1238
- Simpson, C. 1998, *MNRAS*, 297, L39
- Springel, V., Di Matteo, T., & Hernquist, L. 2005, *MNRAS*, 361, 776
- Stasińska, G., Vale Asari, N., Cid Fernandes, R., Gomes, J. M., Schlickmann, M., Mateus, A., Schoenell, W., & Sodr e, L., Jr. 2008, *MNRAS*, 391, L29
- Strauss, M. A., et al. 2002, *AJ*, 124, 1810
- Strateva, I., et al. 2001, *AJ*, 122, 1861
- Stoughton, C., et al. 2002, *AJ*, 123, 485
- Tanaka, M. 2011, *PASJ* in press (Paper-I)
- Taniguchi, Y., Shioya, Y., & Murayama, T. 2000, *AJ*, 120, 1265
- Terlevich, R., & Melnick, J. 1985, *MNRAS*, 213, 841
- Thomas, D., Maraston, C., Bender, R., & Mendes de Oliveira, C. 2005, *ApJ*, 621, 673
- Tremaine, S., et al. 2002, *ApJ*, 574, 740
- Tremonti, C. A., et al. 2004, *ApJ*, 613, 898
- Ueda, Y., Akiyama, M., Ohta, K., & Miyaji, T. 2003, *ApJ*, 598, 886
- Valluri, M., Ferrarese, L., Merritt, D., & Joseph, C. L. 2005, *ApJ*, 628, 137
- Veilleux, S., & Osterbrock, D. E. 1987, *ApJS*, 63, 295
- White, R. L., Becker, R. H., Helfand, D. J., & Gregg, M. D. 1997, *ApJ*, 475, 479
- Yan, R., Newman, J. A., Faber, S. M., Konidaris, N., Koo, D., & Davis, M. 2006, *ApJ*, 648, 281
- Yan, R., et al. 2011, *ApJ*, 728, 38
- Yan, R., & Blanton, M. R. 2011, arXiv:1109.1280
- York, D. G., et al. 2000, *AJ*, 120, 1579